Industrial Chemistry & Materials

ROYAL SOCIETY OF CHEMISTRY

REVIEW

View Article Online
View Journal | View Issue

Cite this: *Ind. Chem. Mater.*, 2023, **1**, 60

Recent progress in non-fused ring electron acceptors for high performance organic solar cells

Huanhuan Gao,[a] Chenyang Han,[a] Xiangjian Wan *[b] and Yongsheng Chen *[b]

In recent years, significant progress has been witnessed in organic solar cells (OSCs), which is mainly attributed to the new active layer materials design, especially fused ring acceptors. However, the majority of fused-ring acceptors suffer from complicated synthetic procedures and unsatisfactory reaction yields and thus high preparation cost. It is difficult to reconcile with the necessity for OPVs to demonstrate the low cost advantage compared with other photovoltaic technologies such as silicon or perovskite solar cells, thus significantly limiting the future application of OSCs. Therefore, it is necessary to develop high efficiency but low cost acceptor materials, *i.e.* non-fused ring electron acceptors (NFREAs). In this review, the recent development of NFREAs from the viewpoint of materials design is discussed. In the first and second sections, NFREAs with different central cores are reviewed. Then, the progress of fully non-fused NFREAs is summarized. Finally, an outlook on the remaining challenges to the field is provided.

Keywords: Organic solar cells; Non-fused ring acceptors; Low cost; Intramolecular noncovalent interaction; Large steric hindrance.

Received 30th August 2022,
Accepted 23rd October 2022

DOI: 10.1039/d2im00037g

rsc.li/icm

1 Introduction

As one of the promising green energy technologies, organic solar cells (OSCs) have many merits such as flexibility, light weight, and large-area roll-to-roll printing manufacture.[1–5] Significant progress has been made in OSCs thanks to the new active layer material invention, deep understanding of the mechanism, and device optimization progress. Particularly in recent years, with the introduction and success of non-fullerene acceptors (NFAs), remarkable results with power conversion efficiencies (PCEs) over 19% have been achieved.[6–9] From the viewpoint of chemical structures, A–D–A type acceptors, where "D" and "A" represent the electron donating (D) and electron accepting (A) moieties in the same molecule, *e.g.* ITIC, Y6 and their analogues or derivatives, have proved to be the most successful NFAs. Currently, PCEs of 9–16% for ITIC and its analogues[10–15] and 15–19% for Y6 and its derivatives[16–20] have been achieved. Most A–D–A acceptors have fused-ring molecular backbones, which can give good planarity and rigidity to the acceptors and be helpful to form stable

[a] *College of New Energy, Xi'an Shiyou University, Xi'an, 710065, China*
[b] *State Key Laboratory of Elemento-Organic Chemistry, The Centre of Nanoscale Science and Technology, Key Laboratory of Functional Polymer Materials, Haihe Laboratory of Sustainable Chemical Transformations, College of Chemistry, Nankai University, Tianjin, 300071, China. E-mail: xjwan@nankai.edu.cn, yschen99@nankai.edu.cn*

Huanhuan Gao

Huanhuan Gao received her PhD degree in Materials Science & Engineering under the supervision of Prof. Yongsheng Chen and Prof. Xiangjian Wan from Nankai University, China, in 2019. Currently, she is a lecturer at Xi'an Shiyou University. Her research interests focus on the design and synthesis of organic functional materials and device optimization, especially on small molecule acceptor materials.

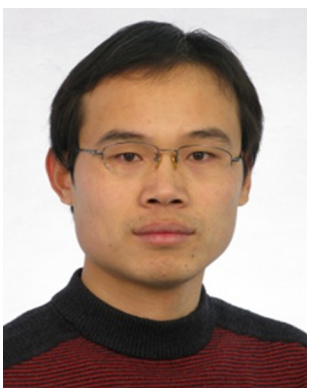

Xiangjian Wan

Xiangjian Wan received his PhD degree in Organic Chemistry from Nankai University, China, in 2006. Currently, he is a professor of Chemistry at Nankai University. His research interests focus on organic functional material design and application, especially on OPV material design and device optimization.

geometric conformation and packing. Despite their excellent properties and device performances, most of the fused-ring acceptors suffer from complicated synthetic procedures and unsatisfactory reaction yields and thus high preparation cost, which will significantly limit the future application of OSCs. In contrast, the price of commercialized silicon-based solar cells has continuously decreased in recent years and low cost is the outstanding advantage of perovskite solar cells. Although OSCs have many unique advantages, their cost issue has to be considered seriously for the commercialization of OSCs. As a result, it is crucial and urgent to design active layer materials from the perspective of not only efficiency but also cost.

To address this issue, much effort has been devoted to designing non-fused ring electron acceptors (NFREAs) in recent years. Compared with that of fused-ring NFAs, the cost of NFREAs can be substantially reduced owing to their simplified synthesis process and generally high yields.[21–23] However, unlike fused-ring acceptors with rigid and planar structures, the conjugated backbones of NFREAs are connected *via* C–C single bonds, which are not favourable to form planar and efficient conjugated structures. Thus, the delocalization of π electrons will be weakened owing to the twisted conformation between the adjacent units, which is unfavourable for the intramolecular charge transfer (ICT). Moreover, the efficient molecular packing will also be influenced owing to the unstable molecular conformations of NFREAs. With this, the PCEs of NFREA-based devices are much lower especially in the early stage. To conquer the unstable conformation problem of NFREAs, researchers have proposed many molecular design methods, which can be roughly divided into two categories. One is to introduce intramolecular non-covalent bonds such as O···S, O···H, F···H, F···S, *etc.* to form conformational locks.[24–26] With the intramolecular noncovalent interaction, the rotation of the C–C single bond can be limited and rigid and coplanar structures can be obtained.[27] The other is to introduce bulky side chains such as alkylbenzene, diarylamine, 2,4,6-triisopropyl benzene, *etc.* to form stable conformation owing to the steric effect.[28] Currently, with the careful molecular design, significant progress has been made for NFREA-based OSCs and PCEs over 15% have been achieved just recently.[28,29]

Yongsheng Chen

Prof. Yongsheng Chen received his PhD in Chemistry from the University of Victoria in 1997. Since 2003, he has been a Chair Professor at Nankai University. His main research interests focus on carbon-based nanomaterials and organic functional materials for green energy applications.

There have been some excellent reviews for NFA materials including fused-ring acceptors and NFREAs.[1,21,30] With the continued rapid progress in the study of NFREAs, it is necessary to have a review with the updated results focusing on the molecular design and correlation between the chemical structures and device performance, which is expected to provide helpful guidance for higher performance material design and device optimization. As shown in Fig. 1, the state-of-the-art NFREAs can be roughly divided into two chemical architectures, *i.e.*, A–π–D–π–A or A–π–A′–π–A, where D and A′ are the electron donating or accepting central core units, π is the conjugated linkage, and A is the electron accepting end groups. In fact, the above two types of NFREAs have a similar design rationale to fused ring acceptors using A–D–A architectures. The difference is whether fused ring backbones or fused ring building blocks are utilized or not in the molecular design. In this review, we will discuss the recent development of NFREAs for OSCs from the views of materials design in the past five years. In the first and second sections, NFREAs with different central cores and π-bridges will be reviewed. Then, the progress of fully non-fused NFREAs will be summarized. Finally, the challenges and perspectives of NFREAs will be provided.

2 NFREAs with electron donating cores

As shown in Fig. 1, the central core with electron-donating or electron-withdrawing abilities plays a critical role in the molecular properties of NFREAs such as absorption, energy levels, and packing modes.[31,32] In particular, coplanar and rigid skeletons of NFREAs could be obtained *via* the intramolecular noncovalent interaction between the core and its adjacent units and/or the bulk steric hindrance of the substituents on the cores. In this and the next sections, we will discuss NFREAs from the views of central cores, *i.e.*, electron donating and electron accepting central cores.

2.1 Benzene core

With its simple chemical structure and ease of functionalization, the benzene unit has been preferably used as a central unit to design NFREAs. In 2018, Chen *et al.* reported an unfused NFA named DF-PCIC with 2,5-difluorobenzene (DFB) as the central core (Fig. 2).[33] DF-PCIC showed a planar skeleton owing to the F···H noncovalent interaction between the central core and the cyclopentadithiophene (CPT) π-bridge. Furthermore, the 2-ethylhexyl side chain in the CPT π-bridge can effectively suppress excessive self-aggregation. Using PBDB-T as a donor, the OSC device achieved a high PCE of 10.12%, with a high open-circuit voltage (V_{oc}) of 0.91 V, a fill factor (FF) of 0.72 and a short-circuit current density (J_{sc}) of 15.66 mA cm^{-2}. It is worth noting that the device PBDB-T:DFPCIC showed good thermal stability with around 70% remaining of the original PCEs upon thermal treatment at 180 °C for 12 h.

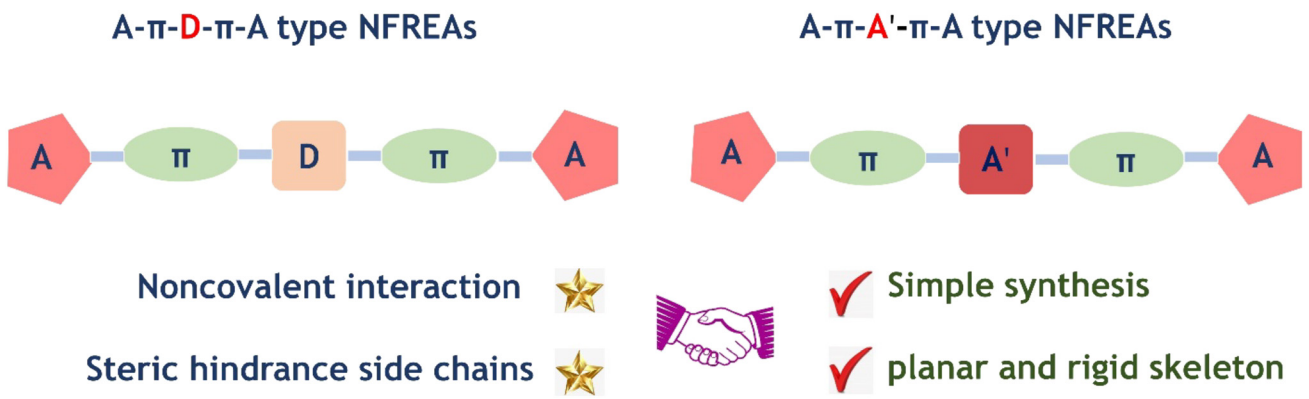

Fig. 1 Illustration of A–π–D–π–A or A–π–A′–π–A type NFREAs and the corresponding design strategies.

Subsequently, in order to explore the effect of different substituents on the central benzene unit, Chen *et al.* designed three NFREAs based on DF-PCIC.[34] When introducing two methoxyl groups (HFO–PCIC) or two fluorine atoms (OF–PCIC) on the DFB unit, the ICT effects were weakened and the two molecules HFO–PCIC and OF–PCIC exhibited blue-shifted absorption in comparison with the control molecule HF–PCIC. According to the geometry analysis (Fig. 3), HF–PCIC possessed a dihedral angle of 14.20° between the CPT π-bridge and the central DFB unit. For HFO–PCIC, two π-bridges kept still at the same level, while the benzene core rotated along one direction, leading to a dihedral angle of 12.36° between the CPT bridge and the benzene core unit. In contrast, OF–PCIC demonstrated a planar backbone with a negligible dihedral angle of 0.05°. As depicted in the crystal of the model compound, 2,2′-(2,5-difluoro-3,6-dimethoxy-1,4-phenylene)dithiophene (FPTO) (-Fig. 3b–d), the fluorine and oxygen atoms choose to approach the hydrogen atoms and the sulfur atoms, respectively, indicating that the structures with F···H noncovalent interaction might be the preferable conformational structures in the above acceptors with the DFB central core. With PBDB-TF (also named PM6) as a donor, PCEs of 11.49%, 8.36% and 9.09% were obtained for HF–PCIC, HFO–PCIC and OF–PCIC based OSCs, respectively.

Peng *et al.* developed two isomer NFREAs (DTP-out-F and DTP-in-F) by introducing 5,5-bis(4-hexylphenyl)-5*H*-dithieno[3,2-*b*:2′,3′-*d*]pyran (DTP) acting as a π-bridge.[35] The results revealed that the isomerization had a great impact on the molecular packing behaviors. DTP-in-F exhibited predominantly face-on orientation, but DTP-out-F exhibited preferable edge-on orientation. Although these two molecules deliver similar optical characteristics, DTP-in-F showed both improved HOMO and LUMO energy levels. As a result, compared with the DTP-out-F based device with a low PCE of 3.97%, the DTP-in-F based device generated a higher PCE of 10.66% with simultaneously enhanced J_{sc} of 18.54 mA cm^{-2}, V_{oc} of 0.91 V and FF of 0.632.

In 2020, our group designed a series of A–D–A type NFREAs incorporating a benzene core substituted with different length alkyloxy side chains to study the relationship between the material structures and morphology and its effects on the device PCE and stability.[36] It was demonstrated that a delicate balance of molecular aggregation and ordered stacking morphology was required to achieve high efficiency and stability. Thus, among those acceptors, UF-EH-2F, with both optimal length and steric hindrance of side chains, achieved the preponderant morphology, where the "efficient state" and "stable state" morphologies are almost overlapped, thus leading to both the highest PCE of 13.56% with the polymer J52 as a donor and the best stability (5% loss after 1368 h when stored in a glovebox without encapsulation), which is the best performance of NFREA-based OSCs when it was reported. The results indicate that it is highly possible to achieve the morphology state required for both high efficiency and stability simultaneously by fine-tuning the chemical structure of active materials for organic solar cells. Bo *et al.* also reported the same acceptor with the name of DOC2C6-2F and achieved a similar PCE of 13.24% with the polymer PBDB-T as a donor.[37] It is thought that the S···O interactions, which have been used for designing high performance organic semiconductor materials with a planar skeleton structure,[38] between the central 2,5-bis(alkyloxy)phenylene unit and two CPT units are the driving force to produce the coplanar molecular skeleton. Thus, the acceptor displayed a broad absorption range and high electron mobilities. In addition, the morphology of blend films could be readily optimized *via* end group modulation. Using the skeleton of the above acceptor UF-EH-2F, Huang *et al.* designed three acceptors named as BN-0F, BN-2F and BN-4F, with gradually increasing degree of fluorination of π-extended end-groups.[39] It was demonstrated that the photoelectric properties, charge transport and morphology of the three acceptors could be modulated by the noncovalent intramolecular S···O interaction and fluorinated π-extended end groups. Finally, an impressive PCE of 14.53% was obtained for the BN-2F based devices.

Tang *et al.* designed NFREAs named DBD-4F and DBT-4F by dissecting the corresponding fused-ring acceptors to investigate the relationship between structures and properties.[40] From the DFT calculation results, the asymmetric linking bridge molecule DBT-4F shows a relatively high degree of coplanarity thanks to the intramolecular noncovalent interaction, but the symmetric acceptor DBD-4F delivered a large dihedral angle of

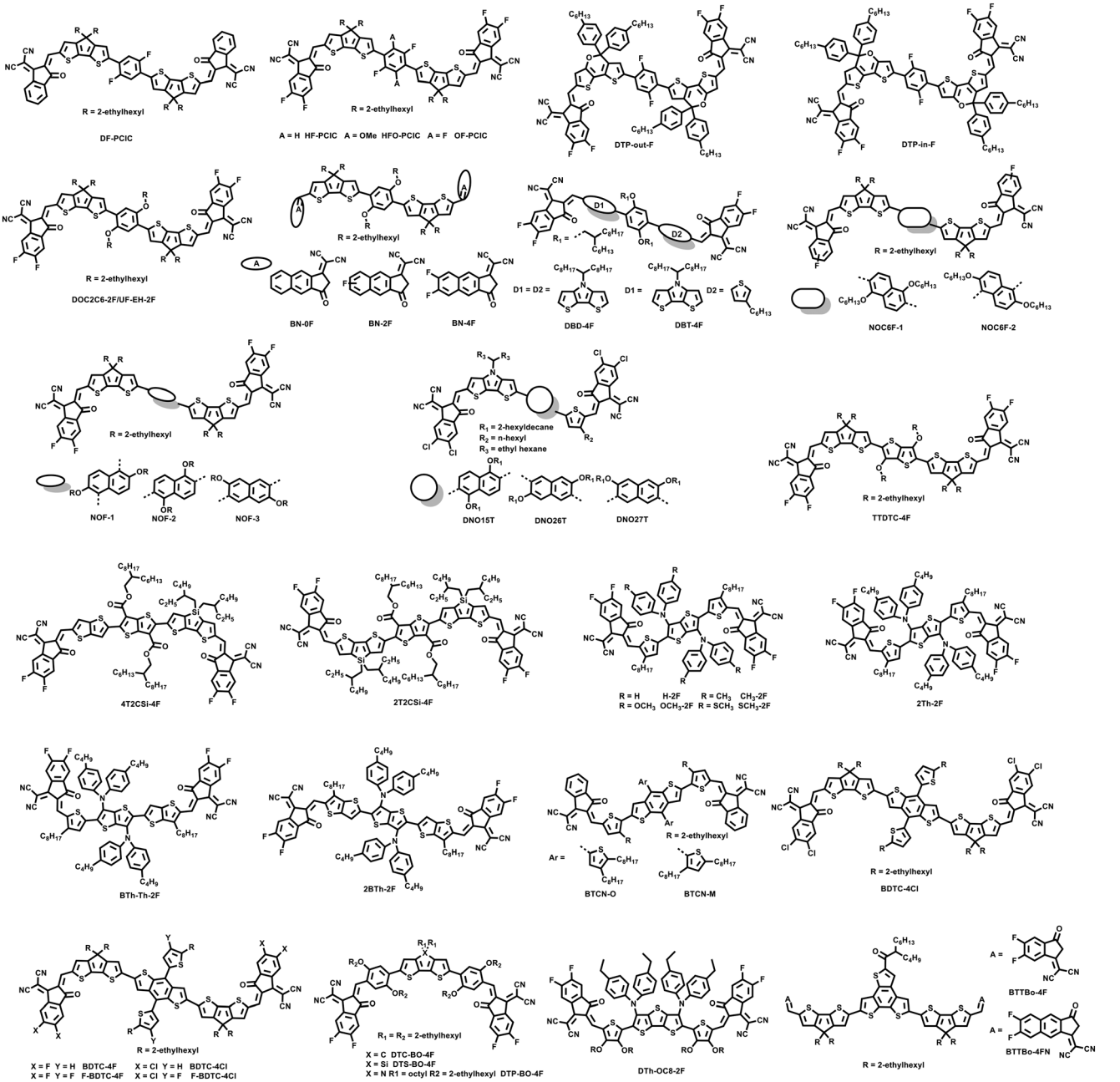

Fig. 2 Chemical structures of electron-donating core-based NFREAs.

21.04°. Moreover, the asymmetric molecule exhibits a larger diploe moment (1.6761 Debye) than the symmetric DBD-4F (0.0141 Debye). Finally, the resultant DBT-4F based device achieved a PCE of 12.14% with a V_{oc} of 0.88 V and an FF of 0.702, higher than the DBD-4F (8.34%) based device. The performances of the above-mentioned related NFREA based OSCs are summarized in Table 1.

2.2 Naphthalene core

With the success of benzene core based acceptors, the naphthalene unit with extended conjugation has also been introduced as the central core to design NFREAs. Bo *et al.* designed two isomeric acceptors NOC6F-1 and NOC6F-2 with the naphthalene core linked with CPT bridges at the 2,6- and 1,5-positions, respectively.[41] This small difference of the two acceptors could largely affect their molecular configuration, packing and OSC performances. Among them, NOC6F-1 exhibited smaller distortions and enhanced π–π stacking compared with NOC6F-2. Therefore, the blend film of PBDB-T:NOC6F-1 showed more ordered π–π stacking both in the out-of-plane (OOP) and in-plane (IP) directions and achieved a higher PCE of 10.62% with a higher J_{sc} of 17.08 mA cm^{-2} and FF of 0.658. Meanwhile the poor planarity NOC6F-2 only

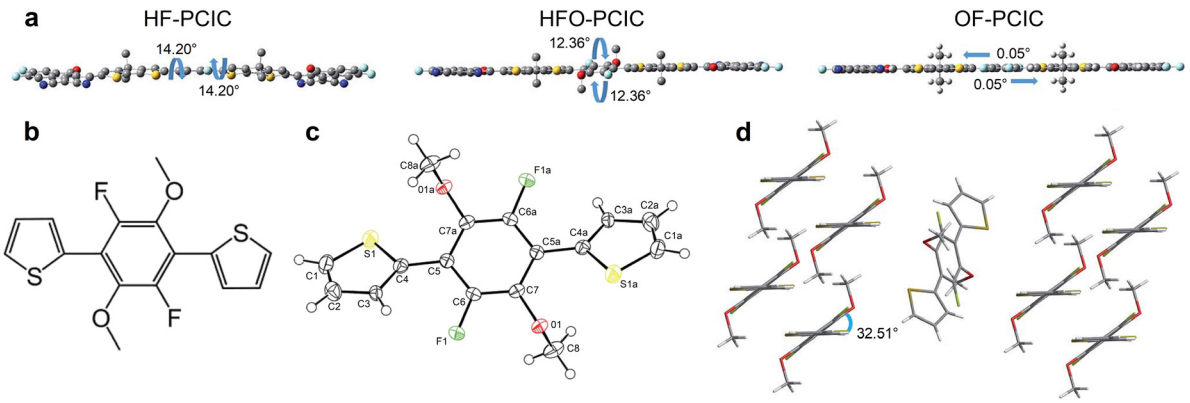

Fig. 3 (a) Molecular geometries of HF–PCIC, HFO–PCIC and OF–PCIC acceptors. (b) Chemical structure of model compound FPT-O. (c) Single crystal structure of FPT-O. (d) Molecular packing (reprinted with permission from ref. 34 Copyright 2018 The Royal Society of Chemistry).

Table 1 The photovoltaic parameters of A–π–D–π–A type NFREA-based devices

NFREAs	HOMO (eV)	LUMO (eV)	E_g (eV)	V_{oc} (V)	J_{sc} (mA cm^{-2})	FF	PCE (%)	Ref.
DF-PCIC	−5.49	−3.77	1.72	0.91	15.66	0.72	10.14	33
HF–PCIC	−5.53	−3.83	1.70	0.91	17.81	0.71	11.49	34
DTP-out-F	−5.61	−3.96	1.65	0.86	10.16	0.45	3.97	35
DTP-in-F	−5.53	−3.92	1.61	0.91	18.54	0.63	10.66	35
UF-EH-2F	−5.49	−4.11	1.38	0.79	24.87	0.69	13.56	36
DOC2C6-2F	−5.49	−3.83	1.66	0.85	21.35	0.73	13.24	37
BN-2F	−5.39	−3.99	1.40	0.813	25.25	0.71	14.53	39
DBT-4F	−5.67	−3.87	1.80	0.88	19.65	0.70	12.14	40
DBD-4F	−5.55	−3.74	1.81	0.88	15.92	0.59	8.34	40
NOC6F-1	−5.55	−3.77	1.78	0.95	17.08	0.66	10.62	41
NOF-3	−5.55	−3.77	1.78	0.898	18.49	0.70	11.58	42
DNO15T	−5.75	−3.94	1.81	0.89	18.95	0.63	10.72	43
DNO26T	−5.57	−3.95	1.62	0.87	18.43	0.62	9.92	43
TTDTC-4F	−5.21	−3.75	1.46	0.57	22.52	0.62	7.81	44
2T2CSi-4F	−5.70	−3.84	1.86	0.84	19.50	0.61	10.04	45
CH_3-2F	−5.59	−4.01	1.58	0.77	22.76	0.70	12.28	46
2BTh-2F	−5.55	−3.98	1.57	0.90	23.61	0.72	15.44	29
BDTC-4Cl	−5.35	−3.75	1.60	0.864	18.56	0.59	9.54	49
F-BDTC-4Cl	−5.59	−3.90	1.69	0.841	19.28	0.64	10.28	50
DTC-BO-4F	−5.59	−3.83	1.76	0.83	22.77	0.70	13.26	51
DTh-OC8-2F	−5.48	−3.90	1.58	0.85	23.65	0.70	14.13	52
BTTBo-4FN	−5.48	−3.86	1.62	0.84	19.56	0.70	11.60	53
Cl-4Cl	−5.58	−3.91	1.67	0.832	20.07	0.65	10.88	55
DCB-4F	−5.50	−3.86	1.64	1.00	16.42	0.58	9.56	54

provided a relatively low PCE of 6.74%. Subsequently, Huang *et al.* reported a series of 2,6-α-, 1,5-β-, and 3,7-β-type naphthalene based NFREAs to regulate the electronic properties, molecular packing and OSC performances *via* the isomeric effects.[42] With the more balanced charge mobility, improved exciton dissociation, low charge recommendation and optimal blend film morphology, the 3,7-β-type naphthalene functionalized NOF-3 based device delivered a high PCE of 11.58%. Tang *et al.* also designed three NFREAs DNO15T, DNO26T and DNO27T with alkoxyl substituted naphthalene as the central core unit and CPT as the bridge, and 2-(5,6-dichloro-3-oxo-2,3-dihydro-1*H*-inden-1-ylidene) malononitrile (IC-2Cl) as the end group.[43] There existed a large difference in the molecular geometry, packing and morphology in the blends with polymer donors owing to the isomerization. DNO15T and DNO26T with low molecular distortions and good coplanar backbones exhibited compact π–π and ordered stacking, thus leading to improved charge transfer and low charge recombination. As a consequence, the DNO15T and DNO26T based devices generated PCEs of 10.72% and 9.92%, respectively, higher than the DNO27T based device (4.32%).

2.3 TT core

In order to broaden the absorption range, Li *et al.* designed a narrow band gap NFREA TTDTC-4F by introducing a strong electron-donating thieno[3,2-*b*]thiophene (TT) unit as the central core.[44] TTDTC-4F possessed a narrow bandgap of 1.25 eV with an absorption edge around 1000 nm. After device optimization, the P3HT:TTDTC-4F based device achieved a PCE of 7.81% with a higher J_{sc} of 22.5 mA cm^{-2}. Recently,

Chen *et al.* designed two NFREAs 2T2CSi-4F and 4T2CSi-4F using diester-thieno[3,2-*b*]thiophene as the central core and 4,4-di-2-ethylhexyl-dithieno[3,2-*b*:2′,3′-*d*]silole (DTSi) or the TT unit as the conjugated linking bridge.[45] It was revealed that the ester side chain can form multiple intramolecular S···O conformational locks, thus generating enhanced molecular packing. Compared with the asymmetric 4T2CSi-4F based device, the symmetric 2T2CSi-4F based device achieved a high PCE of 10.04%, which is mainly due to the red-shifted absorption, enhanced crystallinity and favourable packing and blend film morphology.

In 2021, Bo *et al.* designed four NFREAs (H-2F, CH_3-2F, OCH_3-2F and SCH3-2F) by introducing diphenylamine as the flanking group on the central TT unit in order to improve the solubility and suppress excessive aggregation.[46] It was found that the substituent group at the diphenylamine unit had a great impact on the absorption and energy level of these acceptors, electron mobility and morphology of blend films. Among them, CH_3-2F could form an ordered molecular stacking and a face-on orientation and provided the highest PCE of 12.28%. In their next work, Bo *et al.* designed three NFREAs, 2Th-2F, BTh-Th-2F and 2BTh-2F with the TT core bearing two bis(4-butylphenyl)amino substituents, 3-octylthiophene or 3-octylthieno[3,2-*b*]thiophene as the π bridge.[29] The three acceptors displayed quite similar absorption behaviours in both dilute chloroform and thin film and their molar extinction coefficients gradually increased with increasing π-conjugation length. Moreover, from the single-crystal X-ray diffraction results (Fig. 4), 2Th-2F shows a twisted dihedral angle of 27.61° between the TT core and the thiophene linking bridge. In contrast, 2BTh-2F exhibits a nearly coplanar configuration with a small dihedral angle of 12.17° between the TT core and its adjacent TT π bridges, which is mainly attributed to the presence of intramolecular S···N and S···O interactions. Most importantly, compared with the 2D packing of 2Th-2F, 2BTh-2F demonstrates a 3D network molecular packing, which could provide more electron transport channels and decrease the exciton binding energy and energy loss. Finally, the PBDB-T:2BTh-2F-based OSC showed a PCE of 14.53%, much higher than those of 2Th-2F (11.00%) and BTh-Th-2F (12.87%) based devices. A PCE of 15.44% was achieved for

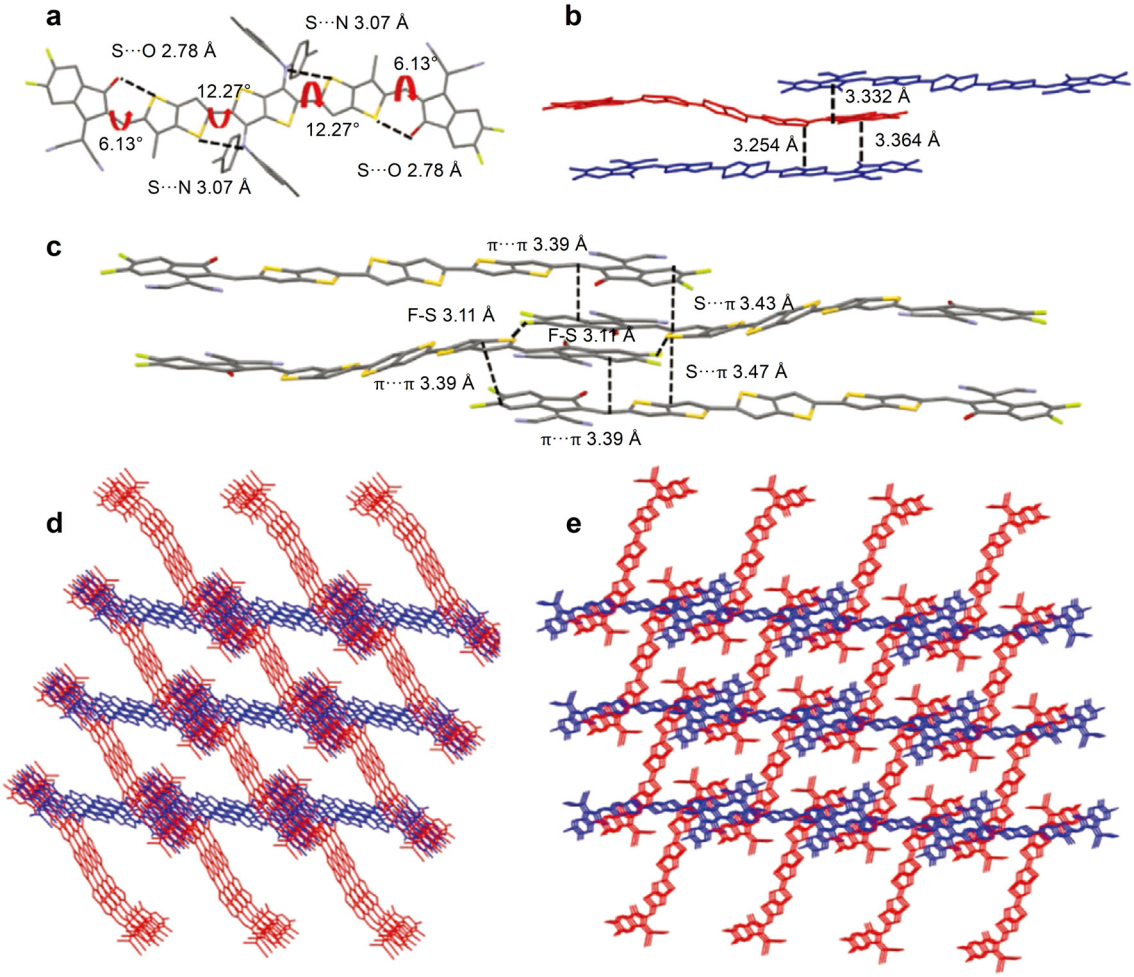

Fig. 4 (a) The single-crystal structure of 2BTh-2F; (b) the face-to-face distance in the triclinic system; (c) the intermolecular interactions between adjacent molecules; (d) 3D molecular packing along the *b*-crystallographic axis; (e) 3D molecular packing along the *c*-crystallographic axis (reprinted with permission from ref. 29 Copyright 2021 Willey-VCH).

the 2BTh-2F-based device when D18 was used as the donor polymer, which is currently the highest efficiency for NFREA-based devices.

2.4 BDT core

The benzodithiophene (BDT) unit is an excellent building block for organic semiconductor material design, which has been widely used in the design of polymer and small molecule materials including donors and acceptors.[47] Hou *et al.* reported two A–D–A type molecules BTCN-M and BTCN-O, which had identical backbones but different substitution positions of alkyl chains on the thiophene of the central BDT unit.[48] It has been demonstrated that the steric hindrance caused by the nonconjugated alkyl in their central units plays a critical role that affects their electron donating and accepting properties. With PBDB-T as a donor, the devices of BTCN-M and BTCN-O showed PCEs of 5.89% and 1.62%, respectively. When blended with $PC_{71}BM$, BTCN-M and BTCN-O also demonstrated very different photovoltaic performances with PCEs of 0.29% and 6.68%. Clearly, the steric hindrance for intermolecular π–π interaction in the central units plays a critical role in the electron donating and accepting properties of A–D–A type molecules. Low steric hindrance on the backbones favours formation of ordered lamellar structures and compact π–π stacking in the solid film for A–D–A type molecules, which can make them act as electron donors. Meanwhile A–D–A molecules with high steric hindrance in the backbones will prefer to pack in ordered structures *via* the interaction between the electron withdrawing end groups, which can make them act as electron acceptors.

In 2019, our group designed and synthesized two NFREAs named BDTS-4Cl and BDTC-4Cl, which used BDT as the central core (D), dithienosilole (DTS) or CPT as the linking bridge, and IC-2Cl as the end group.[49] The synthetic route of the two acceptors was as simple as only a two-step procedure. The PBDB-T:BDTC-4Cl based device demonstrated a PCE of 9.54%, which was much higher than the PCE of 3.73% of the BDTS-4Cl-based device. With $PC_{71}BM$ as a third component, the ternary device PBDB-T:BDTC-4Cl:$PC_{71}BM$ delivered a PCE of 12.19%. Following the above work, we recently have designed four acceptors named BDTC-4F, BDTC-4Cl, F-BDTC-4F, and F-BDTC-4Cl to investigate the effect of synergistic halogenation of the backbone and end group on the photovoltaic performances.[50] Among them, F-BDTC-4Cl with backbone fluorination and end group chlorination achieved a PCE of 10.28%, which is higher than those of the other three acceptors BDTC-4F-(9.70%), BDTC-4Cl-(9.42%), and F-BDTC-4F-(8.84%) based devices.

2.5 Other cores

Besides the central cores mentioned above, other cores with extended conjugation have also been introduced as the central units to design NFREAs. For example, Bo *et al.* reported three NFREAs named DTC-BO-4F, DTS-BO-4F and DTP-BO-4F with a tricyclic fused-ring as the core unit and two 2,5-bis-(alkyloxy)phenylene spacers acting as π-bridges.[51] The multiple intramolecular noncovalent interactions between the π-bridge and the central core or end group such as O···H and S···O can promote a good coplanar geometry and effective charge transport. Among them, DTC-BO-4F exhibited a more red-shifted absorption spectrum and provided a high PCE of 13.26%. Recently, inspired by the success of diarylamine side chains, Bo *et al.* designed a NFREA named DTh-OC8-2F.[52] Firstly, the existence of intramolecular S···O noncovalent interaction guaranteed the molecular orientation and good planarity. Secondly, the large steric hindrance of diarylamine side chains can improve the solubility and suppress single bond rotation. Thirdly, the C-shaped molecule DTh-OC8-2F can effectively reduce excessive aggregation. Finally, a promising PCE of 14.13% was achieved. Huang *et al.* designed two NFREAs BTTBo-4F and BTTBo-4FN using benzotrithiophene (BTT) as the central unit.[53] With the extended conjugation end group, BTTBo-4FN exhibited stronger absorption, a narrower optical bandgap, and more ordered face-to-face p-stacking compared with BTTBo-4F. As a result, the OSC based on BTTBo-4FN showed a higher PCE of 11.60% than the BTTBo-4F-based device (8.27%). Tang *et al.* introduced 7*H*-dibenzo[*c*,*g*]carbazole (DCB) as the central unit and designed a NFREA named DCB-4F.[54] The binary device PM6:DCB-4F showed a PCE of 9.56%. With further device optimization, a PCE of 11.17% was achieved by incorporating 10 wt% $PC_{71}BM$ in the above binary devices. The related photovoltaic parameters discussed above are summarized in Table 1.

3 NFREAs with electron-accepting cores

Besides the electron donating central cores such as benzene, naphthalene, BDT, *etc.*, electron-withdrawing units such as benzothiadiazole (BT), benzotriazole (BTz), quinoxaline (Qx), thieno[3,4-*c*]pyrrole-4,6-dione (TPD), benzo-[1,2-*c*:4,5-*c*′] dithiophene-4,8-dione (BDD), and pyrazine (PZ) have also been used to design NFREAs with the A–π–A′–π–A structure.

As shown in Fig. 5, Huang *et al.* reported two NFREAs, BTCIC and BTCIC-4Cl, by introducing the BT unit as the central core.[56] The two NFAs possess coplanar backbones and broad absorption spectra. The absorption of BTCIC and BTCIC-4Cl was extended to the near-infrared range with onsets at 908 and 946 nm, corresponding to optical band gaps of 1.36 and 1.31 eV, respectively. PCEs of 9.3% and 10.5% were achieved for the BTCIC and BTCIC-4Cl based devices with PBDB-T as the donor. Subsequently, Bo *et al.* designed three acceptors BT-IC4F, BT2F-IC4F and BTOR-IC4F and investigated the substituent effects on the central BT units with a fluorine atom or alkoxy side chain.[57] For BT2F-IC4F and BTOR-IC4F, the intramolecular noncovalent interactions of F···S and O···S favoured construction of ladder-like planar molecular backbones. Particularly for BTOR-IC4F, two alkoxyl chains on the central benzothiadiazole unit could improve the molecular solubility and upshifted its LUMO energy level, and optimize the

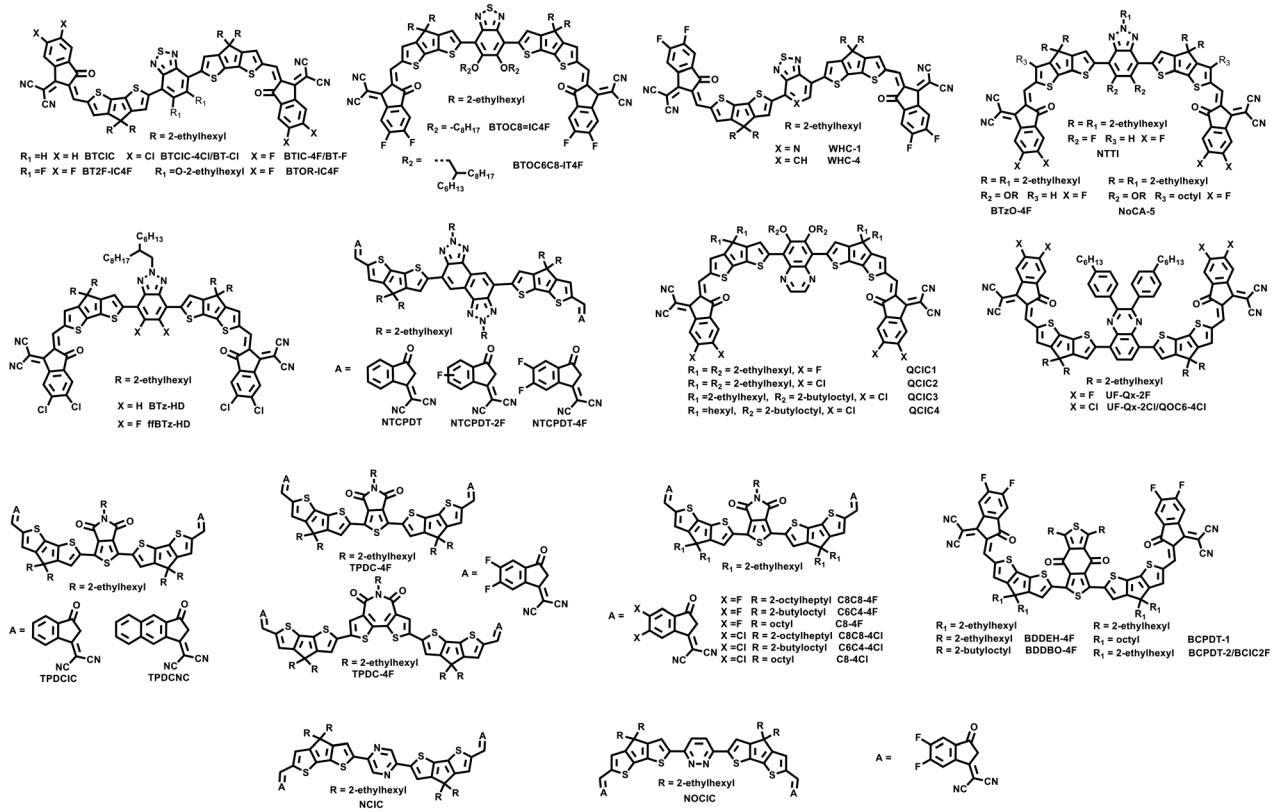

Fig. 5 Chemical structures of electron-accepting core-based NFREAs.

morphology of the active layer. Thus, the PBDB-T:BTOR-IC4F based OSC exhibited a PCE of 11.48%, which is higher than those of the PBDB-T:BT-IC4F (9.83%) and PBDB-T:BT2F-IC4F (8.45%) based devices. Wei and co-workers also designed similar acceptors, BTOC8-IC4F and BTOC6C8-IC4F.[58] They all showed a nearly coplanar molecular geometry owing to the intramolecular S···O interaction. Moderate PCEs of 5.81% and 7.55% were obtained for the BTOC8-IC4F and BTOC6C8-IC4F based devices, respectively. Recently, Choi *et al.* reported a NFREA named WHC-1 using pyridothiadiazole (PT) as the central unit. Compared with the control acceptor WHC-4 with BT as the central core, WHC-1 exhibited downshifted HOMO and LUMO energy levels owing to the strong withdrawing ability of the PT unit, which can decrease the device V_{oc}. Thus, when using PM6 as a donor, the device of WHC-1 showed a lower PCE of 6.6% than the WHC-4 based device (9.3%), which is mainly attributed to the lower V_{oc} of the WHC-1 based device.[59]

Compared with the BT unit, the BTz unit shows a relatively weak electron-withdrawing ability and can provide an additional functionalization site on the 2-position of the triazole.[18] Thus the energy levels, solubilities and packing modes of the molecules incorporating the BTz unit can be efficiently modulated. In 2020, Chen *et al.* reported two NFREAs named NTI and NTTI with two fluorine atoms substituted BTz as the central core.[60] Compared with NTI with thiophene as the linking unit, NTTI with the π-extension CPT bridge exhibited red-shifted absorption and upshifted HOMO and LUMO energy levels. The PBDB-T:NTI-based device showed a poor PCE of 0.45% due to its very low J_{sc} and FF (1.88 mA cm^{-2} and 0.33). A moderate PCE of 8.61% was achieved for PBDB-T:NTTI. Recently, Huang *et al.* also designed acceptor ffBTz-2T with fluorinated BTz as the central core and IC-2Cl as the end group.[61] Due to the formation of intramolecular F···S noncovalent interaction, ffBTz-2T adopted a slip and compact molecular packing structure, while the control molecule BTz-2T with the BTz core without fluorine substitution possessed a cross stacking. As a consequence, the ffBTz-HD based OSC obtained a higher PCE of 10.56% than the BTz-HD based device (8.50%).

Subsequently, Huang *et al.* designed a NFREA named BTzO-4F *via* incorporating the BT central core substituted with two alkoxy chains and CPT linking bridges.[62] As shown in Fig. 5, BTzO-4F possesses a planar geometry owing to the intramolecular N···H and O···S interactions. Thus, a strong π–π stacking could be formed in the pure and blend solid films. Finally, a high PCE of 13.8% was obtained for the device with PBDB-T as the donor. In their following work, Huang *et al.* designed the acceptor NoCA-5 *via* introducing an octyl chain on the outer thiophene ring of the CPT unit.[63] The introduction of the side chain can effectively suppress the rotation of the end group and enhance its molecular rigidity and π–π stacking. With introduction of the side chains, the molecular rigidity and intermolecular π–π stacking were enhanced compared with the control acceptor BTzO-4F. Ultimately, the NoCA-5 based device with J52 as the donor achieved a record PCE of 14.82%

(certified 14.5%). In contrast, the control device J52:BTzO-4F delivered a PCE of 11.71%.

The naphthobistriazole (NT) unit is a good electron withdrawing building block with extended conjugation used to design highly efficient polymer donors. Recently, Li *et al.* designed a series of NFREAs by introducing NT as the central unit.[64] Fluorine atoms were introduced into the IC end groups to tune the physical and crystalline properties of the acceptors. Among them, NTCPDT-4F with two fluorine atoms on each IC group exhibited the highest PCE of 10.79% owing to its higher exciton dissociation efficiency, enhanced charge mobility and lower recombination loss. In contrast, the NTCPDT and NTCPDT-2F based devices only obtained relatively low PCEs of 6.19% and 8.08%, respectively.

Qx has been widely used in donor–acceptor (D–A) copolymers and achieved a high PCE of over 17% for fused-ring acceptor based OSCs.[38,65] Chen *et al.* reported four NFREAs named QCIC1, QCIC2, QCIC3 and QCIC4, which possessed similar molecular conjugated backbones, *i.e.* the Qx central core, CPT bridge and IC end groups, but different side chains on the Qx and CPT units, and halogen atom substitutions on the end groups.[66] Among them, QCIC3 with the 2-butyloctyloxy side chain on CPT and chlorine atom substitution on the IC end group demonstrated the strongest π–π stacking and the preferable phase separation domains, thus yielding the highest PCE of 10.55%. Using the aryl substituted Qx building block as the central core, Chang *et al.* designed two NFREAs UF-Qx-2F and UF-Qx-2Cl.[67] It was revealed that UF-Qx-2Cl exhibited more red-shifted absorption, enhanced crystallinity, more ordered molecular packing and better stability than the UF-Qx-2F based devices. Finally, a PCE of 10.81% was achieved for the J51:UF-Qx-2Cl based device. Zhu *et al.* also reported the same acceptor named QOC6-4Cl.[68] A slightly higher PCE of 12.32% was obtained when blended with the polymer PBDB-T as the donor.

The TPD unit is also a good electron withdrawing building block widely used to design D–A polymers by copolymerization with other donor units. The molecular planarity and rigidity are expected to be enhanced owing to the intramolecular O···S interactions between oxygen atoms of carbonyl groups on TPD and sulfur atoms of adjacent thiophene. In 2019, Chen *et al.* used TPD as the central core unit to synthesize two acceptors, TPDCIC and TPDCNC.[69] TPDCIC and TPDCNC showed good planar molecular backbones owing to the O···H or O···S intramolecular noncovalent interactions with absorption edges of 822 and 852 nm, respectively. When blended with PBDB-T, the TPDCIC and TPDCNC based devices showed PCEs of 9.80% and 10.12%, respectively. By replacing the end group IC of TPDCIC with IC-2F, Kyaw *et al.* designed acceptor TPDC-4F, which demonstrates a smaller optical bandgap of 1.42 eV, a downshifted energy level and ordered molecular packing in pure film.[70] When paired with a much deeper HOMO energy level polymer donor PM6, the resultant device provided a high PCE of 13.35% with a higher J_{sc} of 22.19 mA cm^{-2} and an enhanced FF of 0.706. In their following work, Kyaw *et al.* designed six acceptors based on the above acceptor TPDC-4F by tuning the side chains and end groups.[71] The six acceptors showed a considerable difference in the device performance in spite of the small difference in the side chains and halogenated end groups. Among them, C8C8-4Cl showed the lowest HOMO level, highest electron mobility and most intense molecular packing. The PM6:C8C8-4Cl based device achieved the best PCE of 14.11% with a J_{sc} of 23.8 mA cm^{-2}, a V_{oc} of 0.818 V and an FF of 0.725 owing to its efficient charge transport and preferable morphology. Moreover, the device PM6:C8C8-4Cl showed promising stability with 91.1% of the initial PCE remaining after being placed in air with 67% relative humidity for 50 days.

The BDD unit has been used to construct D–A copolymers, such as PBDB-T, PM6, PM7 *etc.*[47] In 2021, Chen *et al.* adopted a ligand-free direction heteroarylation method to synthesize two simple NFREAs with only three steps using the BDD unit as the central core unit.[72] BDDEH-4F and BDDBO-4F had different lengths of side chains on their BDD units. The two acceptors exhibited similar optical and electrochemical properties in spite of the different side chains on the central BDD units. With PM6 as the donor, BDDEH-4F with 2-ethylhexyl side chains exhibited a PCE of 12.59% with a high J_{sc} of 22.57 mA cm^{-2} owing to the more balanced carrier mobilities and suitable phase separation compared with BDDBO-4F with a PCE of 9.80% and a J_{sc} of 19.09 mA cm^{-2}. Meanwhile, Geng and Jen *et al.* also reported the same acceptor BDDEH-4F and similar acceptors with the same skeleton but a different alkyl chain on the CPT unit.[73,74] PCEs around 10% were obtained for the devices with PBDBT-T as the donor. Recently, Kyaw *et al.* fabricated a ternary device using ambipolar NFREA BDC-4F-C8 with the BDD core as the third component in the binary device PM6:C8C8-4Cl.[75] The HOMO and LUMO energy levels of BDC-4F-C8 lie between PM6 and C8C8-4Cl, which can form the cascaded energy level alignments as well as efficient charge transport and multiple transfer routes. After device optimization, the binary device PM6:BDC-4F-C8 generated a PCE of 12.14%. Due to the optimized morphology, enhanced charge transport and suppressed charge recombination, the ternary device PM6:BDC-4F-C8:C8C8-4Cl provided a high PCE of 15.01%.

Besides the electron-withdrawing central core units discussed above, Chen *et al.* designed two NFREAs, NCIC and NOCIC, utilizing electron-withdrawing group PZ or pyridazine (PDZ) as the core unit.[76] These two NFREAs were easily synthesized in only three steps with high yields. Due to the formation of N···S or N···H intramolecular interaction between the core and the adjacent CPT units, NCIC and NOCIC demonstrated a preferred planar geometry with dihedral angles of merely 0.004° and 0.008°, respectively. Finally, the NCIC and NOCIC based devices delivered PCEs of 10.32% and 9.89%, respectively. The photovoltaic parameters of A–π–A′–π–A type NFREA based devices discussed in this section are summarized in Table 2.

As discussed in the above two sections, regardless of choosing the electron-donating cores or electron-accepting

Table 2 The photovoltaic parameters of A–π–A′–π–A type NFREA-based devices

NFREAs	HOMO (eV)	LUMO (eV)	E_g (eV)	V_{oc} (V)	J_{sc} (mA cm^{-2})	FF	PCE (%)	Ref.
BTCIC-4Cl	−5.64	−4.12	1.52	0.75	21.0	0.66	10.5	56
BT2F-IC4F	−5.98	−4.31	1.67	0.67	19.43	0.65	8.45	57
BTOR-IC4F	−5.92	−4.23	1.69	0.80	20.57	0.69	11.48	57
WHC-4	−5.49	−4.10	1.39	0.75	21.34	0.57	9.37	60
NTTI	−5.83	−3.83	2.00	0.80	17.08	0.63	8.61	60
ffBTz-HD	−5.71	−4.09	1.62	0.86	19.5	0.63	10.56	61
BTzO-4F	−5.45	−3.88	1.57	0.839	23.58	0.70	13.80	62
NoCA-5	−5.43	−3.83	1.60	0.814	26.02	0.70	14.82	63
NTCPDT-4F	−5.58	−3.65	1.93	0.86	20.01	0.63	10.79	64
QCIC3	−5.52	−3.89	1.63	0.816	19.39	0.67	10.55	66
UF-Qx-2F	−5.53	−3.84	1.69	0.78	21.64	0.62	10.54	67
UF-Qx-2Cl	−5.55	−3.89	1.66	0.76	22.71	0.63	10.81	67
QOC6-4Cl	−5.62	−3.87	1.75	0.782	22.91	0.69	12.32	68
TPDCNC	−5.37	−3.83	1.54	0.80	17.40	0.70	9.80	69
TPDCIC	−5.38	−3.78	1.60	0.83	18.16	0.67	10.12	69
TPDC-4F	−5.83	−3.99	1.84	0.852	22.19	0.71	13.35	70
C8C8-4F	−5.69	−4.00	1.69	0.837	22.70	0.69	13.18	71
C8C8-4Cl	−5.75	−4.02	1.63	0.818	23.80	0.73	14.11	71
C6C4-4Cl	−5.69	−3.99	1.70	0.838	22.81	0.67	12.88	71
BDDEH-4F	−5.57	−3.94	1.63	0.88	22.57	0.63	12.59	72
BDDBO-4F	−5.56	−3.93	1.63	0.87	19.09	0.59	9.80	72
BDC-4F-C8	−5.66	−4.26	1.40	0.895	21.4	0.63	12.14	75
NCIC	−5.65	−3.83	1.82	0.879	17.53	0.667	10.32	76
NOCIC	−5.59	−3.80	1.79	0.907	16.22	0.67	9.89	76

cores, it is necessary to maintain a coplanar and rigid skeleton, and thus form the ordered molecular packing to ensure efficient exciton dissociation and charge transport. To this end, two efficient strategies have been established, *i.e.* the intramolecular non-covalent interaction by introducing suitable heteroatoms in the central core or the linking unit, and the steric hindrance by incorporating bulk side chains in the central core or the connecting unit. It is believed that higher efficiency NFREAs can be designed with the deep understanding of the correlation between the molecular structures and device performance.

4 NFAs with fully non fused backbones

Recently, in order to obtain simpler and more efficient photovoltaic materials, a series of fully non-fused ring acceptors have been reported and a high PCE of 15% has been achieved. As shown in Fig. 6, Zhang *et al.* designed a NFREA named Ph-IC by using alkoxyl benzene and two thiophene units as the central core, which showed a fully non fused backbone.[77] Ph-IC has a very simple chemical structure and coplanar conjugated backbone owing to the intramolecular O···H and S···H noncovalent interactions, which makes Ph-IC exhibit an optical bandgap of 1.62 eV with an absorption edge around 800 nm. When using a wide bandgap polymer PBFTZ as a donor, the Ph-IC based device showed a PCE of 5.68% with a V_{oc} of 0.89 V, a J_{sc} of 12.37 mA cm^{-2} and an FF of 51.5%. Furthermore, Chen *et al.* also reported the same simple unfused acceptor named ICTP.[78] The optimized device based on PBDB-T:ICTP provided a PCE of 4.43% with a V_{oc} of 0.97 V, a moderate FF of 50% and a relatively low J_{sc} of 8.29 mA cm^{-2}.

Subsequently, Chen *et al.* reported three NFREAs, PTICH, PTIC and PTICO, which have the same skeletons as Ph-IC but different alkyl substituted thiophene π bridges and fluoride substituted IC groups.[79] It is worth noting that the rotatable conformations of these acceptors in solution could be restrained into planar and stackable conformations in solid film, which are attributed to the intramolecular O···H interaction between the oxygen on the central benzene and its adjacent thiophene unit, and steric hindrance between alkyl chain substituted thiophene and terminal IC-2F. Therefore, compared with the control acceptor ID-4F with a fused backbone, the three NFREAs exhibited blue-shifted absorption in solution due to the C–C rotation, while showing distinct red shifted absorption spectra in thin films owing to the dense J-aggregation and planar conformation with enhanced ICTs. Among them, the PTIC based device with PM6 as the donor achieved a high PCE of 10.27%, which was higher than that of the ID-4F-based device (6.88%). In addition, the PBDB-TF:PTIC-based device exhibited promising stabilities under continuous illumination, *i.e.* maintained about 70% of its initial PCE for 50 h illumination, which might mainly originate from the chemical structures of these NFREAs without extension-fused rings and tetrahedral sp^3 bridges.

In their following work, Chen and coworkers designed two fully NFREAs, PTB4F and PTB4Cl, in which a two dimensional phenyl side-chain at the β-position of bridge thiophene was introduced in order to bring hindrance to prohibit the rotation of end groups IC-2F and IC-2Cl.[80] According to the single crystallographic study (Fig. 7),

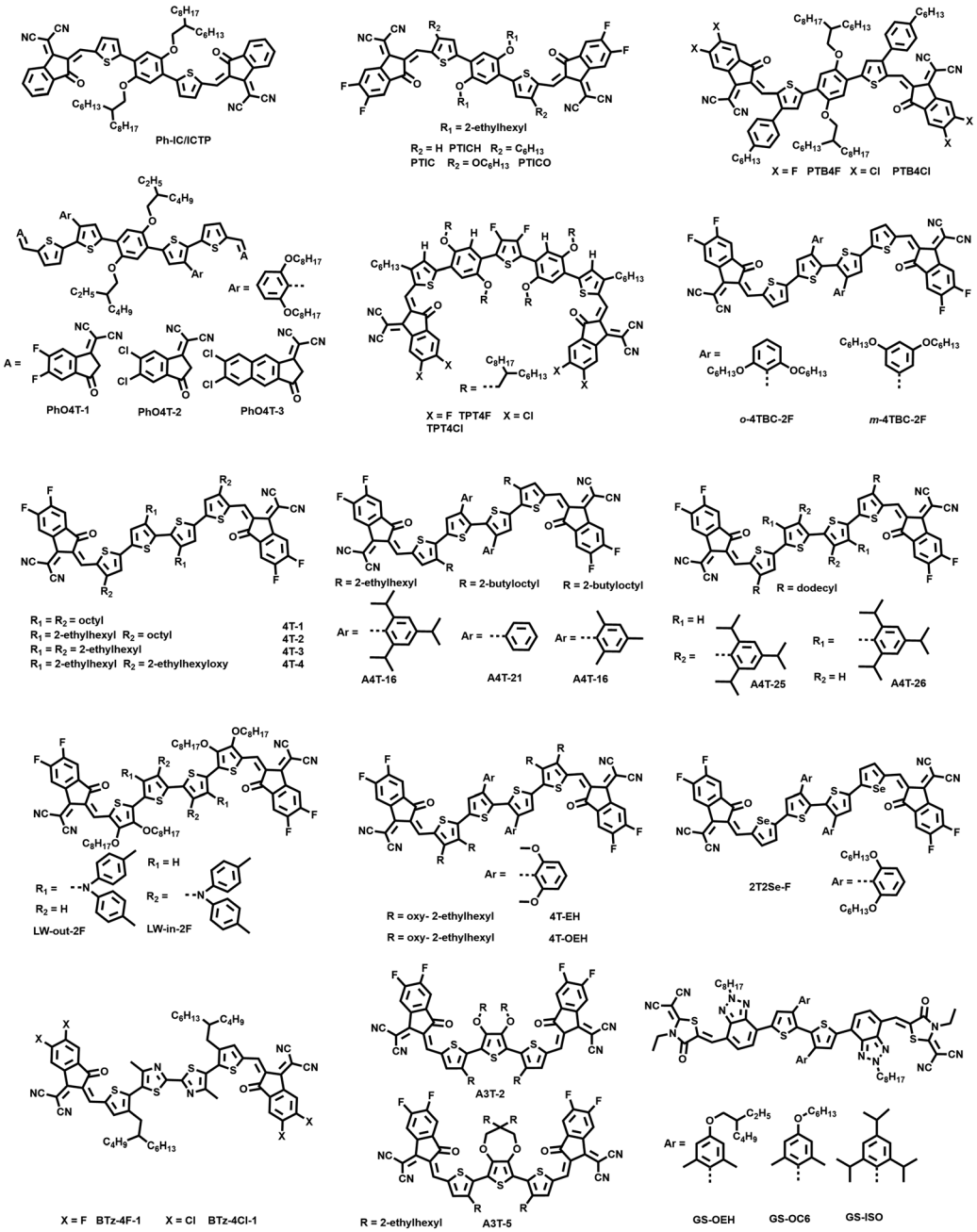

Fig. 6 Chemical structures of the fully NFREAs.

PTB4F and PTB4Cl adopt nearly coplanar conformations, in which the distances between O···S and O···H are shorter than the sum of their van der Waals radius, indicating the presence of intramolecular interactions. Furthermore, the presence of hexylbenzene side chains can regulate the intermolecular stacking, resulting in multiple intermolecular short contacts of $d_{\text{inter,C=O···S}}$ (2.47 Å) and $d_{\text{inter,F···H}}$ (2.66 Å) for PTB4F and $d_{\text{inter,CN···H}}$ (2.62 Å) for PTB4Cl. Finally, the PTB4Cl based device provided a PCE of 12.76%, higher than those of PTIC (10.27%) and PTB4F (7.04%) based devices, indicating the complicated and synergistic effects of side chains and end groups on the molecular properties, morphologies and device performances for these fully NFREAs.

Recently, Huang *et al.* reported three NFREAs, PhO4T-1, PhO4T-2, and PhO4T-3.[81] Compared with the fully NFREAs discussed above, two thiophene units linked by a C–C bond were utilized as π-bridges and 2,6-bis(octyloxy)phenyl was introduced on the thiophene unit adjacent with the alkoxyl benzene central core. The three acceptors also showed planar skeletons owing to the intramolecular noncovalent interactions. The absorption peaks of the PhO4T-1, PhO4T-2, and PhO4T-3 films were red-shifted by around 40, 60 and 50 nm, respectively, compared with those in solutions,

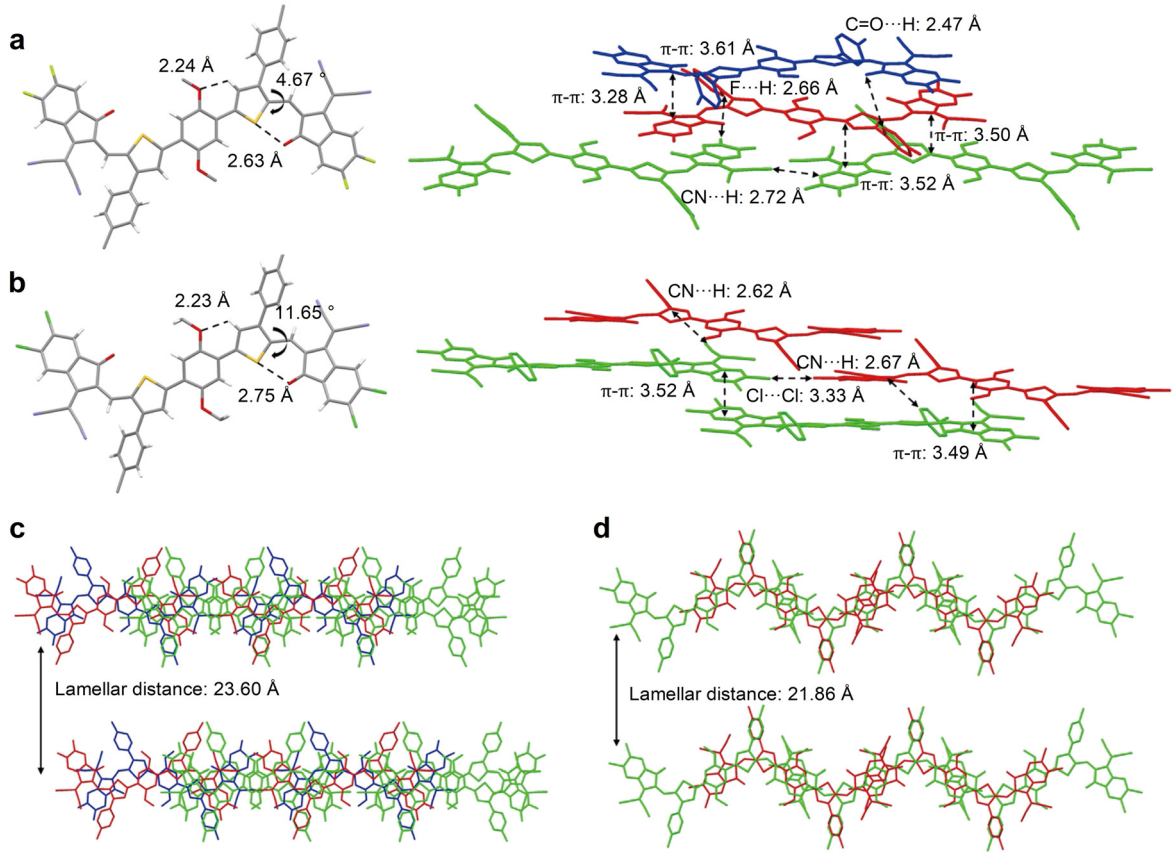

Fig. 7 Molecular conformation and stacking of a) PTB4F and b) PTB4Cl, as well as lamellar diagrams of c) PTB4F and d) PTB4Cl in a single crystal (reprinted with permission from ref. 80 Copyright 2021 Wiley-VCH).

indicating the formation of intense π–π stacking in the solid state. When using PBDB-T as a donor, PhO4T-1 and PhO4T-2 showed PCEs of 9.69% and 11.91%, respectively. As for PhO4T-3 with the π-extension and chlorine substituted end group, a high PCE of 13.76% was achieved.

Li *et al.* reported two simple medium bandgap NFREAs TPT4F and TPT4Cl *via* incorporating multiple intramolecular noncovalent conformational locks to guarantee their planarity and rigidity.[82] TPT4F and TPT4Cl possessed ordered molecular packing and strong photoluminescence in solid films. Finally, the TPT4Cl based device provided a PCE of 10.16%, higher than that of the TPT4F (7.67%) based device. It is noted that the TPT4Cl based device exhibited a relatively narrower bandgap than TPT4F, but showed a higher V_{oc} with a lower non-radiative voltage loss of 0.27 V than the TPT4F-based device.

In 2019, Li and co-workers designed two simple bithiophene core based NFREAs, bearing 1,1-dicyanomethylene-3-indanone as the end group.[83] Although OSCs based on the simple bithiophene NFREA generated a low PCE of 2.4% when combined with PBDB-T, this work demonstrated the potential application of fully NFREAs with simple thiophene backbones. In 2020, Bo *et al.* firstly adopted the quaterthiophene (4T) unit as the backbone to construct two fully NFREAs named *o*-4TBC-2F and *m*-4TBC-2F.[84] The location of hexyloxy chains could significantly influence the molecular planarity, packing and photovoltaic performances. *m*-4BTC-2F displayed a twisted backbone with dihedral angles of the two central thiophene units of 57°, while *o*-4BTC-2F showed a quasi-planar conformation with dihedral angles of 10°. With PBDB-T as the donor, the device *o*-4TBC-2F delivered a PCE of 10.26%, much higher than that of the *m*-4TBC-2F based device (2.63%). In their following work, Bo *et al.* investigated the side chain engineering to fine tune the solubility and molecular packing mode of these 4T backbone based fully NFREAs.[85] The results indicate that the incorporation of 2-ethylhexyl (EH) side chains (4T-3) could enhance the compatibility with the PBDB-T polymer donor. 4T-1 incorporating two linear octyl side chains in the central bithiophene unit exhibited less steric hindrance than those with branched EH side chains. When introducing two branched EH side chains at the central bithiophene unit, 4T-2, 4T-3 and 4T-4 all showed featureless absorption in the solid state, indicating less closed molecular packing structures. Finally, the PBDB-T:4T-3 based device achieved the highest PCE of 10.15%, higher than the 4T-1 (5.53%), 4T-2 (9.09%) and 4T-4 (8.27%) based devices. When using D18 as the donor, a high PCE of 12.04% was afforded for the 4T-3 based OSC.

Recently, Hou *et al.* designed a fully NFREA A4T-16 incorporating 4T backbones with a planar structure and high

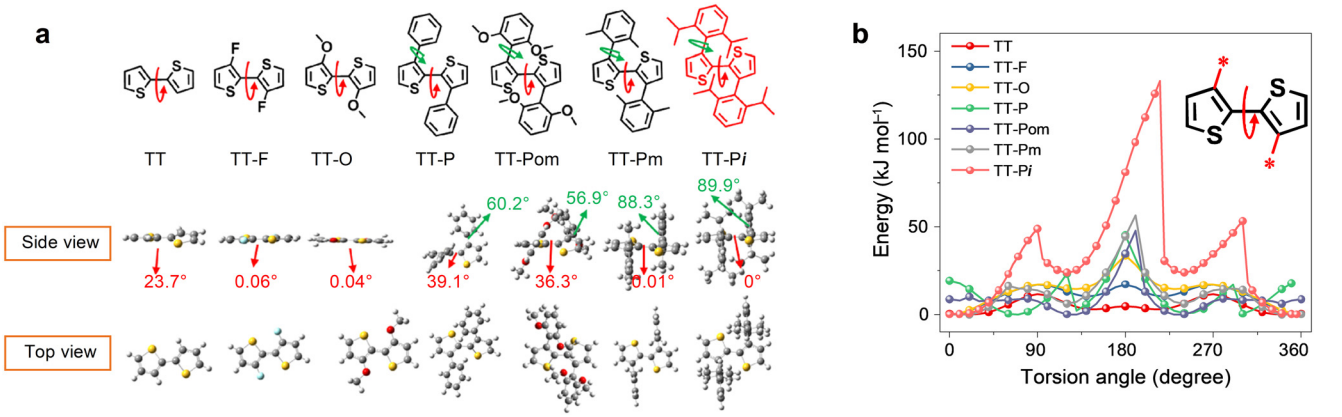

Fig. 8 (a) Chemical structures and DFT calculation results; (b) torsional energy profiles between two thiophenes for several bithiophene units (reprinted with permission from ref. 28 Copyright 2021 Springer Nature).

conformational stability by introducing the functional groups with very large steric hindrance.[28] As the DFT calculation shown in Fig. 8a, owing to the steric hindrance caused by the methyl groups, the dihedral angle between phenyl and thiophene in TT-Pi is 89.9°, and the torsion angle between the two thiophenes is 0°. Moreover, the energy difference between the stable and meta-stable states (ΔEs–ms) and the rotation barrier from the stable state to the meta-stable state (Es → ms) of TT-Pi are 24 and 48 kJ mol^{-1}, respectively, which are much larger than those of the other six 4T derivatives, indicating that the planar bithiophene structure in TT-Pi has very high conformational stability. The single crystal structure of A4T-16 revealed that two adjacent A4T-16 could form a straight linear sub-structure by the end group both in the in-plane and out-of-plane horizontal directions, thus providing two charge transport channels. As a result, the PBDB-TF:A4T-16 based device achieved an outstanding PCE of 15.2% with a J_{sc} of 21.8 mA cm^{-2}, a V_{oc} of 0.876 V and an FF of 0.798, which is much higher than those of the A4T-21 (1.57%) and A4T-23 (10.4%) based devices. Notably, the device based on PBDB-TF:A4T-16 showed good stability with ~84% remaining of its initial efficiencies after 1300 h under simulated AM 1.5 G illumination.

Following their work of A4T-16, Hou *et al.* designed two NFREAs named A4T-25 and A4T-26 by introducing large steric hindrance groups, triisopropyl phenyl, into different positions of the central thiophene units.[86] According to the single crystal analysis, both A4T-25 and A4T-26 exhibit a planar conformation in the central two thiophene units. However, there exists a large dihedral angle of 27.59° for A4T-26 and a relatively small dihedral angle of 12.48° for A4T-25 between the alkyl substituted and central thiophene units. The π–π stacking distances between the end groups for A4T-25 and A4T-26 are 3.51 and 3.18 Å, respectively. A4T-26 displays more compact stacking between its laminar-like secondary structures with a lamellar d-spacing of 4.59 Å, much shorter than that of A4T-25 with a value of 12.92 Å. The calculation on the transfer integrals based on the crystals indicates that electrons can transport effectively in the out-of-plane direction of the π–π stacking in A4T-26, while it is contrary to the case in A4T-25. Therefore, A4T-26 shows an order of magnitude higher electron mobility of 1.44 × 10^{-4} cm^2 V^{-1} s^{-1} than A4T-25. As a consequence, the PBDB-TF:A4T-25 based OSC showed a relatively low PCE of 7.83%, while the PBDB-TF:A4T-26 based device generated a high PCE of 12.1%. Similar results have been obtained in the two fully NFREA isomers LW-in-2F and LW-out-2F reported by Bo *et al.*, in which two diphenylamine side chains were introduced on the outside or inside positions of the central bithiophene units.[87] LW-out-2F with diphenylamine side chains located on the outer side of central bithiophene exhibited a face-on orientation, as well as high and balanced mobility. As a result, the LW-out-2F based device gave a PCE of 12.83%, significantly higher than the LW-in-2F based device with a very low PCE of 0.43%.

With the impressive results of the 4T backbone based acceptors as discussed above, other fully NFREAs have also been designed and achieved promising device performances, which is helpful to understand the correlations between the molecular structures and corresponding properties. For example, Bo *et al.* designed two acceptors 4T-OEH and 4T-EH with 3,4-bis(alkoxy)thiophene and 3,4-dialkylthiophene π-bridge units.[88] 4T-OEH can form a more homogeneous phase morphology and exhibit higher and more balanced hole and electron mobilities compared with 4T-EH. The device based on 4T-OEH can generate a good PCE of 12.12%, which is much higher than that of the 4T-OEH based device (7.36%). Zhang *et al.* reported a selenophene based acceptor 2T2Se-F with near infrared absorption, which achieved a PCE of 12.17%.[89] The weak electron-deficient 4,4′-dimethyl-2,2′-bithiazole was used as the core unit to construct two acceptors BTz-4F-1 and BTz-4Cl-1.[90] When paired with J71, BTz-4F-1 and BTz-4Cl-1 based devices provided PCEs of 5.72% and 3.93%, respectively. Besides the 4T backbone, A3T-2 and A3T-5 with the terthiophene backbone were also designed and provided moderate PCEs of 6.20% and 7.03%, respectively.[91] Recently, Hou *et al.* further modulated the π-linking bridge of 4T based NFREAs by replacing the

Table 3 The photovoltaic parameters of fully NFREA based devices

NFREAs	HOMO (eV)	LUMO (eV)	E_g (eV)	V_{oc} (V)	J_{sc} (mA cm^{-2})	FF	PCE (%)	Ref.
Ph-IC	−5.72	−3.79	1.93	0.89	12.37	0.51	5.68	77
PTIC	−5.59	−3.81	1.78	0.93	16.73	0.66	10.27	79
PTB4F	−5.87	−3.89	1.98	0.94	14.55	0.51	7.04	80
PTB4Cl	−5.91	−3.93	1.98	0.93	19.01	0.72	12.76	80
PhO4T-1	−5.53	−3.94	1.59	0.859	20.71	0.54	9.69	81
PhO4T-2	−5.62	−4.07	1.55	0.841	21.49	0.66	11.91	81
PhO4T-3	−5.58	−4.09	1.49	0.839	23.03	0.71	13.76	81
TPT4F	−5.81	−3.97	1.84	1.00	13.36	0.57	7.67	82
TPT4Cl	−5.90	−3.99	1.91	1.04	15.77	0.62	10.16	82
o-4TBC-2F	−5.63	−4.00	1.63	0.76	20.48	0.66	10.26	84
m-4TBC-2Cl	−5.68	−4.00	1.68	0.84	7.90	0.40	2.63	84
4T-3	−5.85	−3.86	1.99	0.93	18.28	0.71	12.04	85
A4T-16	−5.67	−3.96	1.71	0.876	21.8	0.798	15.2	28
A4T-23	−5.63	−3.98	1.65	0.870	21.0	0.568	10.4	28
A4T-25	−5.56	−3.81	1.75	0.901	17.2	0.50	7.83	86
A4T-26	−5.65	−3.83	1.82	0.885	18.9	0.72	12.1	86
LW-in-2F	−5.59	−3.89	1.70	0.84	22.78	0.67	12.83	87
LW-out-2F	−5.67	−3.92	1.75	0.85	1.64	0.31	0.43	87
4T-OEH	−5.47	−3.94	1.53	0.85	21.78	0.65	12.12	88
4T-EH	−5.54	−3.87	1.67	0.94	13.02	0.53	6.48	88
2T2Se-F	−5.52	−3.83	1.69	0.875	20.63	0.67	12.17	89
BTz-4F-1	−5.88	−3.93	1.95	0.84	12.28	0.55	5.72	90
BTz-4Cl-1	−5.99	−4.03	1.96	0.80	9.66	0.51	3.93	90
A3T-5	−5.84	−4.04	1.80	0.85	15.3	0.54	7.03	91
GS-ISO	−5.51	−3.69	1.82	1.21	13.65	0.70	11.62	92

thiophene π-bridge with the electron-withdrawing BTz unit and synthesized three wide bandgap NFREAs named GS-OEH, GS-OC6 and GS-ISO.[92] Compared with GS-OEH and GS-OC6, GS-ISO demonstrates much stronger crystallinity, thus leading to a smaller energetic disorder, effectively extended exciton diffusion coefficient and higher electroluminescence external quantum efficiency. Therefore, the OSCs based on PBDB-TF:GS-ISO provided a high PCE of 11.62% with a high V_{oc} over 1.2 V. The wide bandgap and high V_{oc} make PBDB-TF:GS-ISO a good front subcell for fabrication of tandem cells. Recently, using PBDB-TF:GS-ISO as a front cell, Hou *et al.* fabricated a tandem cell and achieved an outstanding PCE of 20.2%.[9] The photovoltaic parameters for fully NFREA based OSCs are summarized in Table 3.

To sum up, the fully NFREAs face a greater challenge in controlling the rigid skeleton, since such materials possess more twistable single bonds. Fortunately, the strategy by introducing large steric hindrance has proved to be successful in regulating the rigidity and coplanarity of fully NFREAs. However, most of the OSCs based on the fully NFREAs still show low efficiencies. Thus, it is highly required to conduct more study focusing on the deep understanding of the structure–property relationships for the design of low cost and high efficiency fully NFREAs.

5 Conclusion and perspective

This review has shown the considerable progress of NFREA based OSCs in recent years. Inspired by the A–D–A type fused acceptors and donors, very promising results have been made in recent years for NFREAs, and the initial correlations between the chemical structures and physical properties, morphologies and device performance have been established, which can give valuable guidance for NFREA design with higher efficiencies. It is worth noting that the importance of molecular conformation has been regarded as one of the critical points for NFREA design. Therefore, much attention has been paid to the design of NFREAs with planar and rigid conjugation molecular skeletons. To this end, two general strategies have been developed, *i.e.* intramolecular noncovalent interaction and large steric hindrance. Currently, many NFREAs with rigid and coplanar backbones have been designed mainly utilizing the above strategies, and high PCEs over 15% have been achieved. Despite the promising device results, there are still many issues to be addressed for the design of NFREAs and device fabrication and even their future application. Herein, we provide some perspectives that might offer critical insights to this field.

5.1 NFREA design

Clearly, the recent remarkable progress in NFREAs has mainly been attributed to the NFREA design, which mainly follows the two strategies mentioned above, *i.e.* intramolecular noncovalent interaction and large steric hindrance in order to obtain coplanar and rigid molecular backbones. For new NFREA design, there are some considerations and suggestions as follows. Firstly, it is suggested to further design NFREAs by synergistically utilizing the two strategies and it is necessary to better understand the relationship between the chemical structure and coplanar and rigid skeleton. Undoubtedly, there is great room for molecular design of new NFREAs. Secondly,

NFREAs with architectures other than A–π–D–π–A or A–π–A′–π–A can also be considered, though it seems to be much tougher work. Thirdly, the state-of-the-art NFREAs are small molecules. Considering the promising device performances of polymer acceptors which are designed by the strategy of polymerization of small molecular fused ring acceptors, it might be meaningful to design and evaluate polymer acceptors with non fused ring backbones.

5.2 Donor issue

As discussed in this review, nearly all the OSC based NFREAs are fabricated with only limited several polymer donors, most of which have complex structures that require multi-step synthesis with high costs. We know that donors play the same and important role in determining the OSC performance. In fact, it is also the issue in the whole OSC community that only a few polymer donors show good device performance. Thus, it is necessary and urgent to design polymer donors with both high device performance and low cost. Meanwhile, besides polymer donors, small molecule donors should also be considered to be designed and evaluated with NFREAs. Moreover, it is encouraged to design donors and NFREA materials synergistically from the perspectives of complementary absorption, matched energy levels, preferable miscibility and phase separation, *etc.*

5.3 Morphology control

Morphology control is a critical step to realize high efficiency OSCs. The ideal morphology for OSCs should have suitable donor and acceptor phase separation and interpenetrating structures. To date, various effective morphology control strategies have been invented and established, *e.g.* thermal and/or solvent annealing, additives, and careful molecular modification such as side chain engineering, which have substantially contributed to improve the device efficiencies. Although the established morphology control methods can be directly used in the NFREA based devices, it is necessary to develop new strategies according to the unique properties of NFREAs. In fact, it is still a challenge to well control the active layer morphology and many cases are still investigated in the trial and error way in the OSC community. For NFREAs, their molecular structures with backbones are linked by C–C single bonds and thus unstable conformations should be firstly considered for morphology control since they have negative effects on the molecular packing and blending film morphology.

5.4 Stability

Stability is one of the key issues for all types of OSCs and is determined by many complicated intrinsic and external factors. External factors such as water and oxygen from the air can be well prevented by the sophisticated encapsulation technology that has been used in industry. The intrinsic factors mainly depend on the stability of active layers, including the intrinsic stability of the donor or acceptor, and the morphology stability. To date, most of the donors or acceptors including NFREAs reported in recent years have shown good chemical and thermal stability as well as photo stability. It is worth noting that the double bonds between the central skeletons and the end groups for the widely used A–D–A type or similar type materials might cause possible photoisomerization. Interestingly, a study reported by Li *et al.* indicated that the unfused acceptor PTIC and the photovoltaic device based on it all showed much higher photostability compared with the counterpart fused ring acceptor IT-4F, which is attributed to the structural confinement of PTIC with the hindering outward-chain and planar sp^3 carbon-free backbone.[93] In spite of the promisingly higher stability of NFREAs and their devices, it is suggested to design materials without exocyclic double bonds to avoid the instability issue from the molecular levels. On the other hand, morphology stability has been regarded as another main intrinsic factor for the OSC life. More study is suggested to be conducted during the process of NFREA molecule design and device optimization. It is worth noting that some NFREA-based devices have demonstrated very exciting stability performances, which might originate from the confined conformations and morphologies of NFREAs.

5.5 Cost

The cost of OSC devices is closely related to the price of the active layer material. In spite of their high efficiencies, OSCs based on fused ring acceptors significantly suffer from the high cost of those fused ring acceptors which are synthesized with complex synthesis procedures with multiple steps and unsatisfactory yields. This is the driving force for developing NFREAs. Undoubtedly, with cheap starting materials and simple and only a few synthesis steps, NFREAs have demonstrated substantially decreased cost compared with fused acceptors. It is believed that lower cost and higher efficiency NFREAs will be obtained through further careful molecular design. Meanwhile, the cost of the donor material is also an issue needed to be addressed. Much attention is suggested to be paid to design low cost and high efficiency polymer donors to replace the current ones with high cost. Meanwhile, it is also a good alternative way to develop small molecule donors with simple structures and synthesis procedures.

In summary, to date, promising PCEs over 15% have been achieved for NFREA-based devices, which still fall behind fused acceptor based devices. Compared with the comprehensive investigation of fused acceptors, the study of NFREAs is still in its initial stage. Through further efforts in careful design and synthesis of new NFREAs, together with suitable donor materials design and screening and device morphology control and optimization, it is believed that NFREA OSCs can achieve PCEs close to or even higher than those of fused ring acceptors in the near future. Moreover, from the perspective of industrial application, efficiency, stability and cost are the three key factors that should be carefully considered before one photovoltaic

technology is ready for the commercialization. For NFREA-based OSCs, the efficiencies have reached a remarkable level and will be enhanced in short time. Initial studies on the stability have demonstrated promising results. Low cost is the certain advantage of NFREAs. Therefore, NFREA-based OSCs have demonstrated the very competitive balance of cost, efficiency and stability for industrial application. It is believed that OSCs based on NFREAs will realize commercialization in the near future through further material design and device optimization.

Conflicts of interest

There are no conflicts to declare.

Acknowledgements

The authors gratefully acknowledge the financial support from the Hong Kong Scholar Program (XJ2021-038), the Natural Science Foundation Research Project of Shaanxi Province (Programs No. 2021JQ-595), the National Natural Science Foundation of China (52025033, 21935007), Tianjin City (20JCZDJC00740) and the Postgraduate Innovation and Practical Ability Training Program of Xi'an Shiyou University (YCS21212144).

Notes and references

1 G. Zhang, J. Zhao, P. C. Y. Chow, K. Jiang, J. Zhang, Z. Zhu, J. Zhang, F. Huang and H. Yan, Nonfullerene Acceptor Molecules for Bulk Heterojunction Organic Solar Cells, *Chem. Rev.*, 2018, **118**, 3447–3507.

2 B. Fan, F. Lin, X. Wu, Z. Zhu and A. K. Jen, Selenium-Containing Organic Photovoltaic Materials, *Acc. Chem. Res.*, 2021, **54**, 3906–3916.

3 X. Wan, C. Li, M. Zhang and Y. Chen, Acceptor–donor–acceptor type molecules for high performance organic photovoltaics – chemistry and mechanism, *Chem. Soc. Rev.*, 2020, **49**, 2828–2842.

4 D. Meng, R. Zheng, Y. Zhao, E. Zhang, L. Dou and Y. Yang, Near-Infrared Materials: The Turning Point of Organic Photovoltaics, *Adv. Mater.*, 2022, **34**, 2107330.

5 J. Wang and X. Zhan, From Perylene Diimide Polymers to Fused-Ring Electron Acceptors: A 15-Year Exploration Journey of Nonfullerene Acceptors, *Chin. J. Chem.*, 2022, **40**, 1592–1607.

6 K. Chong, X. Xu, H. Meng, J. Xue, L. Yu, W. Ma and Q. Peng, Realizing 19.05% Efficiency Polymer Solar Cells by Progressively Improving Charge Extraction and Suppressing Charge Recombination, *Adv. Mater.*, 2022, **34**, 2109516.

7 L. Zhu, M. Zhang, J. Xu, C. Li, J. Yan, G. Zhou, W. Zhong, T. Hao, J. Song, X. Xue, Z. Zhou, R. Zeng, H. Zhu, C. C. Chen, R. C. I. MacKenzie, Y. Zou, J. Nelson, Y. Zhang, Y. Sun and F. Liu, Single-junction organic solar cells with over 19% efficiency enabled by a refined double-fibril network morphology, *Nat. Mater.*, 2022, **21**, 656–663.

8 Y. Cui, Y. Xu, H. Yao, P. Bi, L. Hong, J. Zhang, Y. Zu, T. Zhang, J. Qin, J. Ren, Z. Chen, C. He, X. Hao, Z. Wei and J. Hou, Single-Junction Organic Photovoltaic Cell with 19% Efficiency, *Adv. Mater.*, 2021, **33**, 2102420.

9 Z. Zheng, J. Wang, P. Bi, J. Ren, Y. Wang, Y. Yang, X. Liu, S. Zhang and J. Hou, Tandem Organic Solar Cell with 20.2% Efficiency, *Joule*, 2021, **6**, 171–184.

10 Y. Lin, J. Wang, Z. G. Zhang, H. Bai, Y. Li, D. Zhu and X. Zhan, An Electron Acceptor Challenging Fullerenes for Efficient Polymer Solar Cells, *Adv. Mater.*, 2015, **27**, 1170–1174.

11 H.-H. Gao, Y. Sun, X. Wan, X. Ke, H. Feng, B. Kan, Y. Wang, Y. Zhang, C. Li and Y. Chen, A New Nonfullerene Acceptor with Near Infrared Absorption for High Performance Ternary-Blend Organic Solar Cells with Efficiency over 13%, *Adv. Sci.*, 2018, **5**, 1800307.

12 N. Qiu, H. Zhang, X. Wan, C. Li, X. Ke, H. Feng, B. Kan, H. Zhang, Q. Zhang, Y. Lu and Y. Chen, A New Nonfullerene Electron Acceptor with a Ladder Type Backbone for High-Performance Organic Solar Cells, *Adv. Mater.*, 2017, **29**, 1604964.

13 B. Kan, H. Feng, H. Yao, M. Chang, X. Wan, C. Li, J. Hou and Y. Chen, A chlorinated low-bandgap small-molecule acceptor for organic solar cells with 14.1% efficiency and low energy loss, *Sci. China: Chem.*, 2018, **61**, 1307–1313.

14 H. Sun, X. Song, J. Xie, P. Sun, P. Gu, C. Liu, F. Chen, Q. Zhang, Z. K. Chen and W. Huang, PDI Derivative through Fine-Tuning the Molecular Structure for Fullerene-Free Organic Solar Cells, *ACS Appl. Mater. Interfaces*, 2017, **9**, 29924–29931.

15 W. Chen and Q. Zhang, Recent progress in non-fullerene small molecule acceptors in organic solar cells (OSCs), *J. Mater. Chem. C*, 2017, **5**, 1275–1302.

16 J. Yuan, Y. Zhang, L. Zhou, G. Zhang, H.-L. Yip, T.-K. Lau, X. Lu, C. Zhu, H. Peng, P. A. Johnson, M. Leclerc, Y. Cao, J. Ulanski, Y. Li and Y. Zou, Single-Junction Organic Solar Cell with over 15% Efficiency Using Fused-Ring Acceptor with Electron-Deficient Core, *Joule*, 2019, **3**, 1140–1151.

17 K. Jiang, Q. Wei, J. Y. L. Lai, Z. Peng, H. K. Kim, J. Yuan, L. Ye, H. Ade, Y. Zou and H. Yan, Alkyl Chain Tuning of Small Molecule Acceptors for Efficient Organic Solar Cells, *Joule*, 2019, **3**, 3020–3033.

18 F. Qi, K. Jiang, F. Lin, Z. Wu, H. Zhang, W. Gao, Y. Li, Z. Cai, H. Y. Woo, Z. Zhu and A. K. Y. Jen, Over 17% Efficiency Binary Organic Solar Cells with Photoresponses Reaching 1000 nm Enabled by Selenophene-Fused Nonfullerene Acceptors, *ACS Energy Lett.*, 2020, **6**, 9–15.

19 M. Liu, P. Fan, Q. Hu, T. P. Russell and Y. Liu, Naphthalene-Diimide-Based Ionenes as Universal Interlayers for Efficient Organic Solar Cells, *Angew. Chem., Int. Ed.*, 2020, **59**, 18131–18135.

20 M. Liu, Y. Jiang, D. Liu, J. Wang, Z. Ren, T. P. Russell and Y. Liu, Imidazole-Functionalized Imide Interlayers for High Performance Organic Solar Cells, *ACS Energy Lett.*, 2021, **6**, 3228–3235.

21 Q. Shen, C. He, S. Li, L. Zuo, M. Shi and H. Chen, Design of Non-fused Ring Acceptors toward High-Performance, Stable, and Low-Cost Organic Photovoltaics, *Acc. Mater. Res.*, 2022, **3**, 644–657.

22 Y. Li, J. Yu, Y. Zhou and Z. A. Li, Rational Design and Integrative Assembly of Heteromeric Metalla[2]Catenanes Featuring Cp*Ir/Rh Fragments, *Chem. – Eur. J.*, 2022, **28**, 2201675.

23 M. Yang, W. Wei, X. Zhou, Z. Wang and C. Duan, Non-fused ring acceptors for organic solar cells, *Energy Mater.*, 2021, **1**, 100008.

24 Y. Liu, Z. Zhang, S. Feng, M. Li, L. Wu, R. Hou, X. Xu, X. Chen and Z. Bo, Exploiting Noncovalently Conformational Locking as a Design Strategy for High Performance Fused-Ring Electron Acceptor Used in Polymer Solar Cells, *J. Am. Chem. Soc.*, 2017, **139**, 3356–3359.

25 D. Liu, B. Kan, X. Ke, N. Zheng, Z. Xie, D. Lu and Y. Liu, Extended Conjugation Length of Nonfullerene Acceptors with Improved Planarity via Noncovalent Interactions for High-Performance Organic Solar Cells, *Adv. Energy Mater.*, 2018, **8**, 1801618.

26 S. J. Xu, Z. Zhou, W. Liu, Z. Zhang, F. Liu, H. Yan and X. Zhu, A Twisted Thieno[3,4-b]thiophene-Based Electron Acceptor Featuring a 14-π-Electron Indenoindene Core for High-Performance Organic Photovoltaics, *Adv. Mater.*, 2017, **29**, 1704510.

27 Y. Liu, J. Song and Z. Bo, Designing high performance conjugated materials for photovoltaic cells with the aid of intramolecular noncovalent interactions, *Chem. Commun.*, 2021, **57**, 302–314.

28 L. Ma, S. Zhang, J. Zhu, J. Wang, J. Ren, J. Zhang and J. Hou, Completely non-fused electron acceptor with 3D-interpenetrated crystalline structure enables efficient and stable organic solar cell, *Nat. Commun.*, 2021, **12**, 5093.

29 X. Wang, H. Lu, Y. Liu, A. Zhang, N. Yu, H. Wang, S. Li, Y. Zhou, X. Xu, Z. Tang and Z. Bo, Simple Nonfused Ring Electron Acceptors with 3D Network Packing Structure Boosting the Efficiency of Organic Solar Cells to 15.44%, *Adv. Energy Mater.*, 2021, **11**, 2102591.

30 G. Zhang, F. R. Lin, F. Qi, T. Heumuller, A. Distler, H. J. Egelhaaf, N. Li, P. C. Y. Chow, C. J. Brabec, A. K. Jen and H. L. Yip, Renewed Prospects for Organic Photovoltaics, *Chem. Rev.*, 2022, **18**, 14180–14274.

31 F. Liu, Z. Zhou, C. Zhang, T. Vergote, H. Fan, F. Liu and X. Zhu, A Thieno[3,4-b]thiophene-Based Non-fullerene Electron Acceptor for High-Performance Bulk-Heterojunction Organic Solar Cells, *J. Am. Chem. Soc.*, 2016, **138**, 15523–15526.

32 Z. Zhou, W. Liu, G. Zhou, M. Zhang, D. Qian, J. Zhang, S. Chen, S. Xu, C. Yang, F. Gao, H. Zhu, F. Liu and X. Zhu, Subtle Molecular Tailoring Induces Significant Morphology Optimization Enabling over 16% Efficiency Organic Solar Cells with Efficient Charge Generation, *Adv. Mater.*, 2020, **32**, 1906324.

33 S. Li, L. Zhan, F. Liu, J. Ren, M. Shi, C. Z. Li, T. P. Russell and H. Chen, An Unfused-Core-Based Nonfullerene Acceptor Enables High-Efficiency Organic Solar Cells with Excellent Morphological Stability at High Temperatures, *Adv. Mater.*, 2018, **30**, 1705208.

34 S. Li, L. Zhan, W. Zhao, S. Zhang, B. Ali, Z. Fu, T.-K. Lau, X. Lu, M. Shi, C.-Z. Li, J. Hou and H. Chen, Revealing the effects of molecular packing on the performances of polymer solar cells based on A–D–C–D–A type non-fullerene acceptors, *J. Mater. Chem. A*, 2018, **6**, 12132–12141.

35 J. Zhao, X. Xu, L. Yu, R. Li, Y. Li and Q. Peng, Highly Efficient Non-Fused-Ring Electron Acceptors Enabled by the Conformational Lock and Structural Isomerization Effects, *ACS Appl. Energy Mater.*, 2021, **13**, 25214–25223.

36 M. Chang, L. Meng, Y. Wang, X. Ke, Y.-Q.-Q. Yi, N. Zheng, W. Zheng, Z. Xie, M. Zhang, Y. Yi, H. Zhang, X. Wan, C. Li and Y. Chen, *Chem. Mater.*, 2020, **32**, 2593–2604.

37 H. Huang, Q. Guo, S. Feng, C. Zhang, Z. Bi, W. Xue, J. Yang, J. Song, C. Li, X. Xu, Z. Tang, W. Ma and Z. Bo, Noncovalently fused-ring electron acceptors with near-infrared absorption for high-performance organic solar cells, *Nat. Commun.*, 2019, **10**, 3038.

38 C. K. Sun, F. Pan, H. J. Bin, J. Q. Zhang, L. W. Xue, B. B. Qiu, Z. X. Wei, Z. G. Zhang and Y. F. Li, A low cost and high performance polymer donor material for polymer solar cells, *Nat. Commun.*, 2018, **9**, 743.

39 X. Zhang, L. Qin, J. Yu, Y. Li, Y. Wei, X. Liu, X. Lu, F. Gao and H. Huang, High-Performance Noncovalently Fused-Ring Electron Acceptors for Organic Solar Cells Enabled by Noncovalent Intramolecular Interactions and End-Group Engineering, *Angew. Chem., Int. Ed.*, 2021, **60**, 12475–12481.

40 J. Cao, S. Qu, L. Yang, H. Wang, F. Du, J. Yu and W. Tang, Asymmetric simple unfused acceptor enabling over 12% efficiency organic solar cells, *Chem. Eng. J.*, 2021, **412**, 128770.

41 R. Zheng, Q. Guo, D. Hao, C. E. Zhang, W. Xue, H. Huang, C. Li, W. Ma and Z. Bo, Naphthalene core-based noncovalently fused-ring electron acceptors: effects of linkage positions on photovoltaic performances, *J. Mater. Chem. C*, 2019, **7**, 15141–15147.

42 X. Zhang, Y. Wei, X. Liu, L. Qin, N. Yu, Z. Tang, Z. Wei, Q. Shi, A. Peng and H. Huang, Enhancing Photovoltaic Performances of Naphthalene-Based Unfused-Ring Electron Acceptors upon Regioisomerization, *Sol. RRL*, 2021, **5**, 2100094.

43 S. He, Z. Lin, F. Du, X. Wang, Y. Liu and W. Tang, Simple unfused acceptors with optimal naphthalene isomerization enabling 10.72% as-cast organic solar cells, *Chem. Eng. J.*, 2022, **441**, 135973.

44 Z. Liang, X. Cheng, Y. Jiang, J. Yu, X. Xu, Z. Peng, L. Bu, Y. Zhang, Z. Tang, M. Li, L. Ye and Y. Geng, P3HT-Based Organic Solar Cells with a Photoresponse to 1000 nm Enabled by Narrow Band Gap Nonfullerene Acceptors with High HOMO Levels, *ACS Appl. Mater. Interfaces*, 2021, **13**, 61487–61495.

45 J. Zhong, Y. Cui, P. Zhu, M. Zhang, W. Xie, H. Liu, Q. Xie, F. Liu, X. Liao and Y. Chen, Nonfused Ring Electron Acceptors for Efficient Organic Solar Cells Enabled by Multiple Intramolecular Conformational Locks, *ACS Appl. Energy Mater.*, 2022, **5**, 5136–5145.

46 X. Wang, H. Lu, J. Zhou, X. Xu, C. Zhang, H. Huang, J. Song, Y. Liu, X. Xu, Z. Xie, Z. Tang and Z. Bo, High-Performance Simple Nonfused Ring Electron Acceptors with Diphenylamino Flanking Groups, *ACS Appl. Mater. Interfaces*, 2021, **13**, 39652–39659.

47 Z. Zheng, H. Yao, L. Ye, Y. Xu, S. Zhang and J. Hou, PBDB-T and its derivatives: A family of polymer donors enables over 17% efficiency in organic photovoltaics, *Mater. Today*, 2020, **35**, 115–130.

48 D. Liu, L. Yang, Y. Wu, X. Wang, Y. Zeng, G. Han, H. Yao, S. Li, S. Zhang, Y. Zhang, Y. Yi, C. He, W. Ma and J. Hou, Tunable Electron Donating and Accepting Properties Achieved by Modulating the Steric Hindrance of Side Chains in A-D-A Small-Molecule Photovoltaic Materials, *Chem. Mater.*, 2018, **30**, 619–628.

49 Y.-Q.-Q. Yi, H. Feng, N. Zheng, X. Ke, B. Kan, M. Chang, Z. Xie, X. Wan, C. Li and Y. Chen, Small Molecule Acceptors with a Nonfused Architecture for High-Performance Organic Photovoltaics, *Chem. Mater.*, 2019, **31**, 904–911.

50 Y. Wang, S. Liu, H. Gao, L. Wang, W. Wang, B. Zhao, H. Wu and C. Gao, Synergistic halogenation of backbone and end group for high-performance non-fused acceptors based organic solar cells, *Dyes Pigm.*, 2022, **200**, 110178.

51 Y. Zhou, M. Li, N. Yu, S. Shen, J. Song, Z. Ma and Z. Bo, Simple Tricyclic-Based A-π-D-π-A-Type Nonfullerene Acceptors for High-Efficiency Organic Solar Cells, *ACS Appl. Mater. Interfaces*, 2022, **14**, 6039–6047.

52 X. Wang, H. Lu, A. Zhang, N. Yu, G. Ran, Z. Bi, X. Yu, X. Xu, Y. Liu, Z. Tang, W. Zhang, W. Ma and Z. Bo, Molecular-Shape-Controlled Nonfused Ring Electron Acceptors for High-Performance Organic Solar Cells with Tunable Phase Morphology, *ACS Appl. Mater. Interfaces*, 2022, **14**, 28807–28815.

53 S. Ma, Q. Huang, Y. Liang, H. Tang, Y. Chen, J. Zhang, K. Zhang, F. Huang and Y. Cao, Non-fullerene electron acceptors with benzotrithiophene with π-extension terminal groups for the development of high-efficiency organic solar cells, *J. Mater. Chem. C*, 2021, **9**, 13896–13903.

54 F. Du, H. Wang, Z. Zhang, L. Yang, J. Cao, J. Yu and W. Tang, An unfused-ring acceptor with high side-chain economy enabling 11.17% as-cast organic solar cells, *Mater. Horiz.*, 2021, **8**, 1008–1016.

55 Y. Wang, S. Liu, H. Gao, L. Wang, W. Wang, Y. Zhou, B. Zhao, H. Wu and C. Gao, Multiple chlorinations to improve the performance of unfused electron-acceptor based organic photovoltaic cells, *Surf. Interfaces*, 2022, **32**, 102185.

56 S. Pang, X. Zhou, S. Zhang, H. Tang, S. Dhakal, X. Gu, C. Duan, F. Huang and Y. Cao, Nonfused Nonfullerene Acceptors with an A-D-A'-D-A Framework and a Benzothiadiazole Core for High-Performance Organic Solar Cells, *ACS Appl. Mater. Interfaces*, 2020, **12**, 16531–16540.

57 Y. Wang, Z. Liu, X. Cui, C. Wang, H. Lu, Y. Liu, Z. Fei, Z. Ma and Z. Bo, Small molecule acceptors with a ladder-like core for high-performance organic solar cells with low non-radiative energy losses, *J. Mater. Chem. A*, 2020, **8**, 12495–12501.

58 Y. Shi, J. Pan, H. Zhang, C. Yang, Z. Zhang, D. Deng, J. Zhang, K. Lu and Z. Wei, The substituents on the intermediate electron-deficient groups in small molecular acceptors result appropriate morphologies for organic solar cells, *Org. Electron.*, 2021, **93**, 106133.

59 M. D. W. Hussain, H. J. Shin, B. R. Lee, M. Ak, S.-J. Ko, J. Lee and H. Choi, Design of Nonfused Nonfullerene Acceptors Based on Pyrido- or Benzothiadiazole Cores for Organic Solar Cells, *ACS Appl. Energy Mater.*, 2022, **5**, 2202–2210.

60 R. Lv, S. Geng, S. Li, F. Wu, Y. Li, T. R. Andersen, Y. Li, X. Lu, M. Shi and H. Chen, Influences of Quinoid Structures on Stability and Photovoltaic Performance of Nonfullerene Acceptors, *Sol. RRL*, 2020, **4**, 2000286.

61 X. Zhou, S. Pang, B. Wu, J. Zhou, H. Tang, K. Lin, Z. Xie, C. Duan, F. Huang and Y. Cao, Noncovalent Interactions Induced by Fluorination of the Central Core Improve the Photovoltaic Performance of A-D-A'-D-A-Type Nonfused Ring Acceptors, *ACS Appl. Energy Mater.*, 2022, **5**, 7710–7718.

62 X. Liu, Y. Wei, X. Zhang, L. Qin, Z. Wei and H. Huang, An A-D-A'-D-A type unfused nonfullerene acceptor for organic solar cells with approaching 14% efficiency, *Sci. China: Chem.*, 2020, **64**, 228–231.

63 X. Zhang, C. Li, L. Qin, H. Chen, J. Yu, Y. Wei, X. Liu, J. Zhang, Z. Wei, F. Gao, Q. Peng and H. Huang, Side-Chain Engineering for Enhancing the Molecular Rigidity and Photovoltaic Performance of Noncovalently Fused-Ring Electron Acceptors, *Angew. Chem., Int. Ed.*, 2021, **60**, 17720–17725.

64 C. Wang, B. Wang, Y. Wu, S. Liang, L. Yuan, D. Xia, C. Zhao, F. Liu and W. Li, Naphthobistriazole based non-fused electron acceptors for organic solar cells, *J. Mater. Chem. C*, 2022, **10**, 8070–8076.

65 L. Perdigón-Toro, L. Q. Phuong, F. Eller, G. Freychet, E. Saglamkaya, J. I. Khan, Q. Wei, S. Zeiske, D. Kroh, S. Wedler, A. Köhler, A. Armin, F. Laquai, E. M. Herzig, Y. Zou, S. Shoaee and D. Neher, Understanding the Role of Order in Y-Series Non-Fullerene Solar Cells to Realize High Open-Circuit Voltages, *Adv. Energy Mater.*, 2022, **12**, 2103422.

66 S. Ye, S. Chen, S. Li, Y. Pan, X. Xia, W. Fu, L. Zuo, X. Lu, M. Shi and H. Chen, Synergistic Effects of Chlorination and Branched Alkyl Side Chain on the Photovoltaic Properties of Simple Non-Fullerene Acceptors with Quinoxaline as the Core, *ChemSusChem*, 2021, **14**, 3599–3606.

67 M. Chang, Y. Zhang, B.-S. Lu, D. Sui, F. Wang, J. Wang, Y. Yang and B. Kan, The design of quinoxaline based unfused non-fullerene acceptors for high performance and stable organic solar cells, *Chem. Eng. J.*, 2022, **427**, 131473.

68 J. Huang, S. Li, J. Qin, L. Xu, X. Zhu and L. M. Yang, Facile Modification of a Noncovalently Fused-Ring Electron Acceptor Enables Efficient Organic Solar Cells, *ACS Appl. Mater. Interfaces*, 2021, **13**, 45806–45814.

69 S.-Z. Geng, W.-T. Yang, J. Gao, S.-X. Li, M.-M. Shi, T.-K. Lau, X.-H. Lu, C.-Z. Li and H.-Z. Chen, Non-fullerene Acceptors with a Thieno[3,4-c]pyrrole-4,6-dione (TPD) Core for Efficient Organic Solar Cells, *Chin. J. Polym. Sci.*, 2019, **37**, 1005–1014.

70 D. Luo, L. Li, Y. Shi, J. Zhang, K. Wang, X. Guo and A. K. K. Kyaw, Electron-deficient diketone unit engineering for non-fused ring acceptors enabling over 13% efficiency in organic solar cells, *J. Mater. Chem. A*, 2021, **9**, 14948–14957.

71 D. Luo, Z. Jiang, C. Shan, L. Li, C. Duan, Q. Liu, Z. Wang, K. Wang, B. Xu and A. K. K. Kyaw, Simultaneous Tuning of Alkyl Chains and End Groups in Non-fused Ring Electron Acceptors for Efficient and Stable Organic Solar Cells, *ACS Appl. Mater. Interfaces*, 2022, **14**, 24374–24385.

72 Z. Wu, Y. Chen, L. Zhang, D. Yuan, R. Qiu, S. Deng, H. Liu, Z. Zhang and J. Chen, A ligand-free direct heteroarylation approach for benzodithiophenedione-based simple small molecular acceptors toward high efficiency polymer solar cells, *J. Mater. Chem. A*, 2021, **9**, 3314–3321.

73 Q. Wang, K. Huang, Y. Zhang, L. Ye, W. Ni, M. Li and Y. Geng, Near-infrared absorbing non-fullerene acceptors with unfused D-A-D core for efficient organic solar cells, *Org. Electron.*, 2021, **92**, 106131.

74 Y. Li, H. Fu, Z. Wu, X. Wu, M. Wang, H. Qin, F. Lin, H. Y. Woo and A. K. Jen, Regulating the Aggregation of Unfused Non-Fullerene Acceptors via Molecular Engineering towards Efficient Polymer Solar Cells, *ChemSusChem*, 2021, **14**, 3579–3589.

75 D. Luo, Z. Jiang, W. Yang, X. Guo, X. Li, E. Zhou, G. Li, L. Li, C. Duan, C. Shan, Z. Wang, Y. Li, B. Xu and A. K. K. Kyaw, Dual-functional ambipolar non-fused ring electron acceptor as third component and designing similar molecular structure between two acceptors for high-performance ternary organic solar cells, *Nano Energy*, 2022, **98**, 107186.

76 J. Gao, Y. Li, S. Li, X. Xia, X. Lu, M. Shi and H. Chen, Non-fullerene acceptors with nitrogen-containing six-membered heterocycle cores for the applications in organic solar cells, *Sol. Energy Mater. Sol. Cells*, 2021, **225**, 111046.

77 X. Li, Z. Xu, X. Guo, Q. Fan, M. Zhang and Y. Li, Synthesis and photovoltaic properties of a simple non-fused small molecule acceptor, *Org. Electron.*, 2018, **58**, 133–138.

78 Z. Zhang, S. Zhang, Z. Liu, Z. Zhang, Y. Li, C. Li and H. Chen, A Simple Electron Acceptor with Unfused Backbone for Polymer Solar Cells, *Acta Phys.-Chim. Sin.*, 2019, **35**, 394–400.

79 Z. P. Yu, Z. X. Liu, F. X. Chen, R. Qin, T. K. Lau, J. L. Yin, X. Kong, X. Lu, M. Shi, C. Z. Li and H. Chen, Simple non-fused electron acceptors for efficient and stable organic solar cells, *Nat. Commun.*, 2019, **10**, 2152.

80 T.-J. Wen, Z.-X. Liu, Z. Chen, J. Zhou, Z. Shen, Y. Xiao, X. Lu, Z. Xie, H. Zhu, C.-Z. Li and H. Chen, Simple Non-Fused Electron Acceptors Leading to Efficient Organic Photovoltaics, *Angew. Chem., Int. Ed.*, 2021, **60**, 12964–12970.

81 C. Li, X. Zhang, N. Yu, X. Gu, L. Qin, Y. Wei, X. Liu, J. Zhang, Z. Wei, Z. Tang, Q. Shi and H. Huang, Simple Nonfused-Ring Electron Acceptors with Noncovalently Conformational Locks for Low-Cost and High-Performance Organic Solar Cells Enabled by End-Group Engineering, *Adv. Funct. Mater.*, 2021, **32**, 2108861.

82 T.-J. Wen, J. Xiang, N. Jain, Z.-X. Liu, Z. Chen, X. Xia, X. Lu, H. Zhu, F. Gao and C.-Z. Li, Non-fused medium bandgap electron acceptors for efficient organic photovoltaics, *J. Energy Chem.*, 2022, **70**, 576–582.

83 Y. Li, Y. Xu, F. Yang, X. Jiang, C. Li, S. You and W. Li, Simple non-fullerene electron acceptors with unfused core for organic solar cells, *Chin. Chem. Lett.*, 2019, **30**, 222–224.

84 Y.-N. Chen, M. Li, Y. Wang, J. Wang, M. Zhang, Y. Zhou, J. Yang, Y. Liu, F. Liu, Z. Tang, Q. Bao and Z. Bo, A Fully Non-fused Ring Acceptor with Planar Backbone and Near-IR Absorption for High Performance Polymer Solar Cells, *Angew. Chem., Int. Ed.*, 2020, **59**, 22714–22720.

85 Y. Zhou, M. Li, H. Lu, H. Jin, X. Wang, Y. Zhang, S. Shen, Z. Ma, J. Song and Z. Bo, High-Efficiency Organic Solar Cells Based on a Low-Cost Fully Non-Fused Electron Acceptor, *Adv. Funct. Mater.*, 2021, **31**, 2101742.

86 J. Li, H. Li, L. Ma, Y. Xu, Y. Cui, J. Wang, J. Ren, J. Zhu, S. Zhang and J. Hou, Influence of Large Steric Hinderance Substituent Position on Conformation and Charge Transfer Process for Non-Fused Ring Acceptors, *Small Methods*, 2022, **6**, 2200007.

87 H. Lu, X. Wang, S. Li, D. Li, N. Yu, Z. Tang, Y. Liu, X. Xu and Z. Bo, Diphenylamine Substituted High-performance Fully Nonfused Ring Electron Acceptors: The Effect of Isomerism, *Chem. Eng. J.*, 2022, **435**, 134987.

88 X. Zheng, W. Liu, H. Lu, N. Yu, Y. Wang, H. Huang, S. Li, X. Wang, H. Wang, Y. Liu, X. Xu, Z. Tang and Z. Bo, A simple high-performance fully nonfused ring electron acceptor with a planar molecular backbone, *Chem. Eng. J.*, 2022, **444**, 136472.

89 X. Ding, X. Chen, Y. Xu, Z. Ni, T. He, H. Qiu, C.-Z. Li and Q. Zhang, A selenophene-containing near-infrared unfused acceptor for efficient organic solar cells, *Chem. Eng. J.*, 2022, **429**, 132298.

90 J. Guo, W. Tang, Y. Zhang, C. Qian, J. Wang, H. Tan and W. Zhu, Simple non-fused small-molecule acceptors with bithiazole core: synthesis, crystallinity and photovoltaic properties, *Mater. Adv.*, 2022, **3**, 554–561.

91 J. Zhu, C. Yang, L. Ma, T. Zhang, S. Li, S. Zhang, H. Fan and J. Hou, Terthiophene based non-fused electron acceptors for efficient organic solar cells, *Org. Electron.*, 2022, **105**, 106512.

92 P. Bi, S. Zhang, J. Ren, Z. Chen, Z. Zheng, Y. Cui, J. Wang, S. Wang, T. Zhang, J. Li, Y. Xu, J. Qin, C. An, W. Ma, X. Hao and J. Hou, A High-Performance Nonfused Wide-Bandgap Acceptor for Versatile Photovoltaic Applications, *Adv. Mater.*, 2022, **34**, 2108090.

93 Z. X. Liu, Z. P. Yu, Z. Q. Shen, C. L. He, T. K. Lau, Z. Chen, H. M. Zhu, X. H. Lu, Z. Q. Xie, H. Z. Chen and C. Z. Li, Molecular insights of exceptionally photostable electron acceptors for organic photovoltaics, *Nat. Commun.*, 2021, **12**, 3049.